Neural mechanisms of handedness for precision drawing: hand-dependent engagement of cortical networks for bimanual control and tool use

Namarta Kapil[1]*, Taewon Kim[1,2]*, Samah Gassass[1], Ruiwen Zhou[3], Alexandre R. Carter[4], Ian G. Dobbins[5], Lei Liu[3], Mark P. McAvoy[1], Muriah D. Wheelock[6], Yong Wang[7], David M. Brogan[8], Christopher J. Dy[8], Susan E. Mackinnon[9], Benjamin A. Philip[1,6]

*: Co-first authors

1: Program in Occupational Therapy, Washington University School of Medicine, St. Louis MO
2: Kinesiology, Physical Medicine & Rehabilitation, Pennsylvania State University, University Park PA
3: Biostatistics, Washington University School of Medicine, St. Louis MO
4: Neurology, Washington University School of Medicine, St. Louis MO
5: Psychological & Brain Sciences, Washington University, St. Louis MO
6: Radiology, Washington University School of Medicine, St. Louis MO
7: Obstetrics & Gynecology, Washington University School of Medicine, St. Louis MO
8: Orthopedic Surgery, Washington University School of Medicine, St. Louis MO
9: Plastic & Reconstructive Surgery, Washington University School of Medicine, St. Louis MO

Corresponding Author: Benjamin Philip, benjamin.a.philip@gmail.com

Funding: This work was supported by NINDS R01 NS114046 to Benjamin A. Philip. Data storage was funded by NCI grant P30 CA091842 and NCATS grant UL1 TR002345.

ABSTRACT

Neural mechanisms underlying handedness remain poorly understood. We used functional magnetic resonance imaging (fMRI) to study performance of a visually guided drawing task with each hand. We hypothesized that the left superior parietal lobule supports drawing with either hand, and individuals with chroninc peripheral nerve injury (PNI) to the dominant hand use the same mechanism as healthy adults.

Methods: 33 right-handed adults (23 healthy, 10 patients) underwent fMRI while performing a precision drawing task, alternating between the right hand (RH) and left hand (LH). 20 regions of interest (12 a *priori* and 8 post-hoc) were examined for LH>RH effects on BOLD magnitude and on functional connectivity (FC) modulation via generalized psychophysiological interaction.

Results: During LH drawing, contralateral primary motor cortex (M1) had lower magnitude, and greater FC with two networks of equal-or-greater magnitude: left M1-dorsal premotor, and intrahemispheric parieto-temporal network. Contralateral M1 also had reduced interhemispheric FC with inferior parietal lobule, which exhibited lower magnitude. Patient group did not interact with these effects.

Conclusions: Three neural mechanisms differentiate LH from RH drawing. First, a left hemisphere bimanual control network engages intrahemispherically (directly) during RH drawing and interhemispherically (indirectly) during LH drawing. Second, LH drawing increases engagement of a contralateral network that may reflect increased task demands. Third, RH drawing increases engagement of an interhemispheric tool use network. The first and third networks may explain the dominant hand's performance advantages. PNI patients use the same mechanisms, highlighting their potential as a neuromodulatory target to enhance LH performance after RH impairment.

Keywords: Functional laterality, peripheral nerve injury, visuomotor control, functional magnetic resonance imaging, fine motor control

1. INTRODUCTION

Human handedness is a multifactorial construct (Dexheimer et al., 2024), one aspect of which is left-right asymmetries in upper limb performance ("performance asymmetries" for brevity). Little is known about the neural mechanisms underlying these asymmetries, even though they are routinely expressed during our everyday actions. According to the complementary dominance theory (Kitchen et al., 2025; Britne A Shabbott & Robert L Sainburg, 2008), these asymmetries arise from lateralized cortical specializations for different aspects of movement: in right-handed individuals, the left hemisphere contains specializations for precision control of trajectories and predictive dynamics, while the right hemisphere contains specializations for stabilization and impedance control. Each of these lateralized specializations supports bilateral action, but is primarily connected to the contralateral hand, leading to e.g. a right-hand (RH) advantage for smooth trajectories. However, these neural specializations cannot yet be assessed or targeted to support rehabilitation because the specific neural mechanisms of performance asymmetries remain unknown.

Our current understanding of the neural mechanisms underlying performance asymmetries is based on lesion and neuroimaging studies, each of which offer different limitations. Lesion studies have shown that the left hemisphere contains a specialization that supports precision trajectory control with both hands, and is expressed across motor tasks with varying demands; including two-dimensional reaching tasks with complex demands (Schaefer et al., 2012), and simpler tasks such as ballistic two-dimensional reaching (Mani et al., 2013; Schaefer et al., 2009) and finger-tapping sequences (Haaland et al., 2004). However, lesion studies cannot provide anatomical precision due to lesion heterogeneity, nor can they distinguish between stroke-related deficits and post-stroke adaptation. Neuroimaging allows precise spatial measurement, but is often restricted to simpler movements: such studies have identified a role for left M1 in bilateral finger tapping (Hayashi et al., 2008; Tzourio-Mazoyer et al., 2015), increased involvement of ipsilateral M1 under high task demands during two-finger joystick movements (Barany et al., 2020; Buetefisch et al., 2014; Wischnewski et al., 2016), and greater interhemispheric functional connectivity (FC) for the non-preferred hand (NPH) vs. preferred hand (PH) during simple open/close fist movements (Tsurugizawa et al., 2023). Overall, these studies provide important insights but remain limited in their ability to capture the full scope of real-world movement control, as few neuroimaging tasks engage the precision trajectory control that defines the PH's performance advantage, let alone the mechanisms involved in real-world upper limb actions.

Real-world movements—such as writing, using utensils, or reaching in cluttered environments—involve a dynamic integration of feedforward and feedback mechanisms (Kringelbach et al., 2023; Peterson et al., 2021). Investigating the neural basis of these real-world processes necessitates ecologically valid tasks that capture the complexity and variability of natural behavior rather than artificially constrained experimental conditions (Finn et al., 2022; Finn et al., 2020) that predominate much of the existing lesion and neuroimaging literature. This recognition has prompted a growing shift in cognitive neuroscience toward naturalistic functional MRI (fMRI) designs that incorporate dynamic stimuli such as movies, narratives, and virtual reality (Bottenhorn et al., 2018; Saarimaki, 2021; Zhang et al., 2021). These approaches elicit rich, multimodal brain activity and engage distributed neural networks, including regions that remain unrecruited during simpler tasks, leading to deeper insights into real-world cognition (Hasson et al., 2010). Extending this naturalistic approach to motor control research, however, remains challenging in the fMRI environment due to postural constraints and motion-related artifacts (Reddy et al., 2024; Scarapicchia et al., 2017). Despite these challenges, naturalistic motor tasks have been successfully used to elicit distinct activation patterns via real-time visuomotor feedback (Karimpoor et al., 2018; Yang et al., 2024) and reaching and grasping of 3D objects (Freud et al., 2018). These findings

support the need for demanding and ecologically-relevant motor paradigms in fMRI studies to understand the neural basis of lateralized motor control.

The neural mechanisms of handedness hold critical clinical relevance to patients with chronic impairment of the PH. Chronic PH impairment occurs frequently despite surgery and/or rehabilitation, affecting approximately 22% of hemiplegic stroke patients (Stinear et al., 2012) and 22% of patients with upper extremity peripheral nerve injury (PNI) (Dyck et al., 2005; He et al., 2014; Philip et al., 2020). Better outcomes following PH-PNI are associated with improved performance of the NPH (Kim et al., 2024), but strategies to facilitate NPH use during rehabilitation remain poorly understood (Kim et al., 2025; Marcori et al., 2019). Bridging this gap requires a mechanistic understanding of the asymmetric neural mechanisms of naturalistic action. To that end, we developed a fMRI visually-guided precision drawing task (Philip & Frey, 2014; Philip et al., 2023) designed to engage participants in an ecologically relevant activity (control of a pen) that requires both feedforward and feedback control during continuous dynamic movements. Critically, pen control skills have a strong PH advantage in most humans (Blank et al., 2000), and therefore are uniquely impaired in patients with chronic impairment of the PH. By having participants perform this task with their PH and NPH, we aim to isolate the mechanisms that support PH-like action in the NPH – mechanisms that could be targeted to enhance rehabilitation outcomes in individuals with chronic PH deficits.

In the current study, we isolated "PH-like action with the NPH" (in right-handed participants, thus "RH-like action with the LH") via a task fMRI study of participants performing a precision drawing task with each hand (LH and RH, separately). We analyzed blood oxygenation level dependent (BOLD) magnitude via general linear models (GLM), and functional connectivity (FC) via generalized psychophysiological interactions (gPPI). Based on previous work (Philip et. al, 2021), we hypothesized that precision drawing's LH > RH difference ($hand_{LH-RH}$) would entail greater ipsilateral BOLD magnitude in a superior parietal lobule (SPL) locus. In addition, to establish neural correlates for the processes of adapting to chronic PH impairment after neurological injury, we hypothesized that patients with chronic PNI to the RH would use the same neural mechanisms as healthy adults.

2. METHODS

2.1 *Participants*

Thirty-three right-handed adults (24 female; ages 47 ± 18, range 24-82) performed a visually-guided precision drawing task (see *fMRI Task* below) in the fMRI scanner. 10/33 participants had peripheral nerve injuries (PNI) to their right arm ("patients"). Participant demographics are listed in **Table 1** and their clinical characteristics are listed in **Table 2**. Two additional patients were excluded from the current analysis because they were unable to complete the task with their affected RH, and four additional participants were excluded due to poor task compliance or excess motion, as detailed below (see *2.5 Motion Correction and Screening*). These six participants were therefore not included in the final sample (n = 33). Demographic and performance data were stored and managed via the Research Electronic Data Capture system (Harris et al., 2009). All participants gave informed consent, and all procedures were approved by the Institutional Review Board at Washington University in St. Louis School of Medicine.

Participants were recruited based on physician referral, medical record search, community recruitment flyers and email lists, and individuals who contacted the laboratory from e.g. clinicaltrials.gov. Inclusion criteria for all participants were: age ≥ 18, English speaking and reading, MRI compatible, and right handed as determined by self report and Edinburgh Handedness Inventory score ≥ +40 (Oldfield, 1971). Additional inclusion criteria for patients were: a chronic (≥ 6 month) peripheral nerve injury (neuropathy

with specific localized cause) to the hand, arm, or shoulder; and some impairment to writing, defined as both of: (A) score 2+ (Mild+) on the question "How much difficulty have you had in the last week with writing?" from Disabilities of the Arm, Shoulder, and Hand survey (Beaton et al., 2001); and (B) Box and Blocks motor performance ≥ 1 standard deviation below the mean of age-matched healthy adults (Mathiowetz et al., 1985). For all participants, exclusion criteria were: motor function diagnosis affecting RH in past 2 years (or for patients: diagnoses currently affecting RH unrelated to PNI), motor function diagnosis affecting LH in past 2 years, upper extremity surgery in past 2 months, concussion in past 6 months, amputation (affecting any part of thumb, index, or middle fingers), current chemotherapy, or history of PNI-unrelated conditions that affect brain structure or connectivity (e.g. chronic pain, chronic cocaine use, stroke, traumatic brain injury).

Sample size was based on a power analysis using preliminary data (N = 26) (Kim et al., 2023), which showed potential positive $hand_{LH\text{-}RH}$ effects (i.e. LH > RH) in BOLD magnitude in one region of interest (ROI): superior parietal lobule ipsilateral to movement, SPL-ipsi; see *ROI Selection* below) (Mumford, 2012). We conducted a simulation-based power analysis using a linear mixed-effects model with a random intercept for each subject. Fixed effects included behavioral covariates (velocity and direction, modeled separately for each hand or as differences or ratios) and demographic covariates (sex, age, and group). Using the preliminary data to approximate the underlying data-generating mechanism, 500 resampled datasets were generated and the planned analysis was applied to simulated samples of increasing size. Under the effect sizes and variability observed in the pilot data, the results suggested that a sample size of approximately N = 30 would provide 90% power to detect the target effect at a two-sided significance level of $\alpha = 0.05$. As with all pilot-based power calculations, these estimates are conditional on the observed effect sizes and variance structure and should be interpreted as approximate. To accommodate potential participant exclusion we increased the target sample size to N = 39, which led to a final sample of 33 participants as described in the first paragraph of this section.

Table 1: Participant demographics.

	Total (n=33)	**Patient (n=10)**	**Healthy (n=23)**	**Between groups**
Age (y), mean ± SD	48 ± 18	52 ± 17	46 ± 18	t = -0.818, p = 0.424
Sex (female), n (%)	24 (74%)	7 (73%)	17 (74%)	$\chi^2(1) = 0.000$, p > 0.99
Race/Ethnicity, n				Fisher: df = 6, p = 0.900
Native American	1	1	0	
White	22	7	15	
Black	5	1	4	
Asian	3	1	2	
Hispanic and/or Latino	1	0	1	
Middle Eastern/North African	1	0	1	
Prefer not to say	1	0	1	
Education, n				Fisher: df = 2, p > 0.99
High school or equivalent	2	0	2	
Some college	20	7	13	
Post college degree (e.g., Masters)	10	3	7	

Notes: Between-group differences were assessed with independent-sample t tests (continuous data), chi-square (χ^2) tests (categorical data), or Fisher's exact test (multi-category data). All participants had at least a high school education.

Table 2: Patient clinical characteristics.

Clinical Characteristics	Patient (n=10)
Severity, n	
Neurapraxia	6
Axonotmesis	3
Neurotmesis	2
# Surgeries (for this injury)	0.91 ± 0.83
Time since last surgery (mo)	7.60 ± 12.88
Time since injury (mo)	9.55 ± 11.94
Affected nerve, n	
Ulnar	6
Median	5
Radial	2
Other	3
Injury location, n	
Brachial Plexus	2
Elbow	2
Forearm	2
Wrist	7
Hand	2
Nerve transfer surgery = Yes	2 (18%)

Note: Totals may not add to 10 due to multiple injuries/nerves/locations per patient.

2.2 *fMRI Acquisitions*

Scans were performed on a Siemens PRISMA 3T MRI scanner. fMRI BOLD EPIs were collected using a T2*-weighted gradient echo sequence, a standard 64-channel birdcage radio-frequency coil, and the following parameters: TR = 662 ms, TE = 30 ms, flip angle = 52°, 72 x 72 voxel matrix, FOV = 216 mm, 60 contiguous axial slices acquired in interleaved order, resolution: 3.0 x 3.0 x 3.0 mm, bandwidth = 2670 Hz/pixel, multi-band acceleration = 6x. Siemens auto-align was run at the start of each session. High-resolution T1-weighted structural images were also acquired, using the 3D MP-RAGE pulse sequence: TR = 4500 ms, TE = 3.16 ms, TI = 1000 ms, flip angle = 8.0°, 256 x 256 voxel matrix, FOV = 256 mm, 176 contiguous axial slices, resolution: 1.0 x 1.0 x 1.0 mm. A T2-weighted image was also acquired at: TR = 3000 ms, TE = 409 ms, 256 x 256 voxel matrix, FOV = 256 mm, 176 contiguous axial slices, resolution: 1.0 x 1.0 x 1.0 mm. Spin echo field maps were also collected before the functional runs.

2.3 *fMRI Task*

Each participant used a MRI-compatible tablet (**Figure 1A**) to complete six BOLD functional scans while performing a visually guided precision drawing task based on the STEGA app and previous studies of precision drawing in fMRI (Philip & Frey, 2014; Philip et al., 2023). Participants performed the task using one hand per scan, alternating between left and right hand across the six scans (three scans per hand). During the task, participants saw hollow shapes, and were instructed to draw a line within the bounds of the shape (**Figure 1B**), as fast as possible while prioritizing staying in-bounds over speed. To minimize head and shoulder motion, participants were also instructed to draw with only movements of their fingers and hand, while keeping their upper arm and f orearm as still as possible. Participants received real-time visual feedback via a transparent overlay of hand/pen over the shape and drawn line (**Figure 1C**), provided via the tablet's bluescreen technology (Karimpoor et al., 2015; Tam et al., 2011). Pen position data was collected at 60 Hz. The task was presented in a block design with 15.2 seconds (23 images) of drawing, followed by 15.2 seconds (23 images) of rest (fixation cross). A scan comprised ten cycles of draw/rest, with an additional rest block at the start, and 3.3 seconds (5 images) of additional rest after the final rest block, leading to a total duration of 5:23 (488 volumes total: 230 drawing, 258 rest) per scan. Immediately prior to the scan, participants completed 1 scan with each hand in a mock fMRI scanner to familiarize with the task and apparatus, and to practice drawing while keeping their arm still.

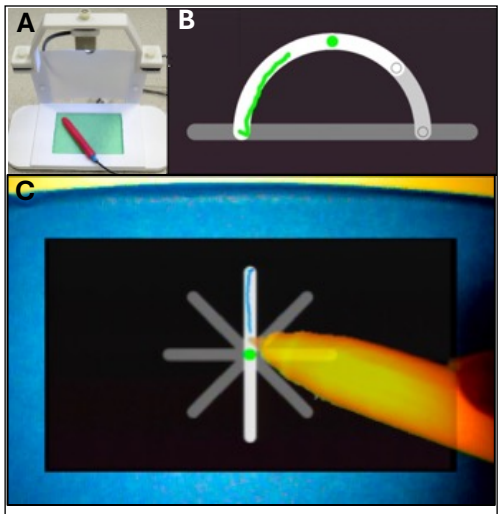

Figure 1: Apparatus and task. **A:** MRI-compatible tablet. **B:** STEGA precision drawing task. **C:** Participant view of bluescreen integration.

2.4 fMRI Preprocessing

The data were preprocessed using *fMRIPrep* 24.1.1(Esteban et al., 2019; RRID:SCR_016216), which is based on *Nipype* 1.8.6 (Gorgolewski et al., 2011; RRID:SCR_002502). Many internal operations of *fMRIPrep* use *Nilearn* 0.10.4 (Abraham et al., 2014; RRID:SCR_001362), mostly within the functional processing workflow.

2.4.1 Anatomical preprocessing*:* The T1-weighted (T1w) volume was corrected for intensity non-uniformity with N4BiasFieldCorrection (Tustison et al., 2010), distributed with ANTs 2.5.3 (Avants et al., 2008; RRID:SCR_004757). The T1w-image was skull-stripped using antsBrainExtraction.sh workflow (using OASIS30ANTs template). The segmentation of cerebrospinal fluid (CSF), white-matter (WM) and gray-matter (GM) was performed on the brain-extracted T1w using fast (FSL, RRID:SCR_002823,(FSL, Zhang et al., 2002; RRID:SCR_002823). Brain surfaces were reconstructed using recon-all (FreeSurfer 7.3.2, Dale et al., 1999; RRID:SCR_001847), and the brain mask was refined by reconciling ANTs- and FreeSurfer-derived segmentations of the cortical gray-matter of Mindboggle(Klein et al., 2017; RRID:SCR_002438). Finally, the T1w volume was normalized to symmetrical MNI standard space (*ICBM 152 Nonlinear Symmetrical template version 2009c* [RRID:SCR_008796; TemplateFlow ID: MNI152NLin2009cSym]) using nonlinear registration with antsRegistration (ANTs 2.5.3), producing an anatomical reference for functional co-registration.

2.4.2 Functional preprocessing: Each of the six BOLD functional runs was motion-corrected by estimating rigid-body transformations to a reference volume using mcflirt (FSL, Jenkinson et al., 2002). The estimated *fieldmap* was then aligned with rigid-registration to the target EPI (echo-planar imaging) reference run. The field coefficients were mapped on to the reference EPI using the transform. The BOLD reference was then co-registered to the T1w reference using bbregister (Freesurfer, Greve & Fischl,

2009). Several confounding time-series were calculated based on the *preprocessed BOLD*: framewise displacement (FD) along with the WM, CSF, and global signal. FD was computed using fsl_motion_outliers (relative root mean square displacement between affines, Jenkinson et al., 2002). The WM and CSF signals were extracted from masks derived from the brain segmentations, and the global signal from the whole brain mask. Three global signals were extracted from CSF, the WM, and the whole-brain masks. Additionally, a set of physiological regressors were extracted to allow for component-based noise correction (CompCor, Behzadi et al., 2007). Principal components were estimated after high-pass filtering the *preprocessed BOLD* time-series (using a discrete cosine filter with 128s cut-off) for the two *CompCor* variants: temporal (tCompCor) and anatomical (aCompCor). tCompCor components were then calculated from the top 2% variable voxels within the brain mask. For aCompCor, three probabilistic masks (CSF, WM and combined CSF+WM) were generated in anatomical space. These masks were resampled into BOLD space and binarized by thresholding at 0.99. The head-motion estimates and CSF, WM, and global signals were expanded with the inclusion of temporal derivatives and quadratic terms for each (Satterthwaite et al., 2013). Additional nuisance timeseries were calculated by means of principal components analysis of the signal found within a thin band (*crown*) of voxels around the edge of the brain, as proposed by Patriat et al. (2017). All resamplings were performed with *a single interpolation step* by composing all the pertinent transformations (i.e. head-motion transform matrices, susceptibility distortion correction when available, and co-registrations to anatomical and output spaces). Gridded (volumetric) resamplings were performed using nitransforms, configured with cubic B-spline interpolation.

2.5 *fMRI Motion Outlier Identification and Screening*

Three methods were used to identify and exclude participants based on motion, task-correlated motion, or poor task compliance. This process evaluated the 37 participants who completed the task, and led to the exclusion of four participants (total) who are therefore not included in the final sample (n = 33). Throughout this process, motion was defined as framewise displacement (FD), calculated at each volume using FSL_motion_outliers (Jenkinson et al., 2012).

To screen participants with high motion, two screening criteria were employed: 1) Participant-level FD threshold: participant-mean FD was calculated by averaging FD within each run, and then averaging across runs for each participant. Participants were removed from analysis if their participant-mean FD was > 0.5 mm (Power et al., 2012; Power et al., 2014); based on this criterion, 1 participant was excluded. 2) Within-participant motion outliers: for each participant, outlier volumes were defined as FD > 75th percentile + (1.5 * inter-quartile range). This threshold identified 4.6% of volumes as outliers (# outlier volumes per scan: range 0-68, mean 22.4, quartiles 10, 20, 33). A participant would be excluded if their # outliers exceeded 20% of the data in any scan (98 volumes), but no participants met that criterion.

To screen participants with excess task-correlated motion, the coefficient of determination (Pearson r^2) was calculated between FD and the task timecourse. Correlation was calculated for each run, and averaged across runs within each participant. These values ranged 0.00004-0.075 (mean 0.021, median 0.016). This process was repeated for the first derivative of the task timecourse, leading to correlation values that ranged 0.001-0.137 (mean 0.047, median 0.033). Participants were excluded from analysis if their correlation value exceeded the outlier threshold of 75th percentile + (1.5 * inter-quartile range) for either the timecourse (threshold r^2 = 0.161) or its derivative (threshold r^2 = 0.239). Based on this criterion, 2 participants were excluded.

To screen participants who failed to comply with the task, a two-step process was used. First, experimenters qualitatively evaluated participant compliance during data collection (a yes/no warning

flag); 7 participants were flagged for follow-up. Second, the flagged participants were explored using objective data for 3 measures of task compliance: number of finger touches (which cause the drawn line to jump across the screen), amount of time spent drawing during drawing blocks (which would be low if the participant was slow to notice the change from rest to draw), and performance (BIS, see *Behavioral Data Analysis* below). One flagged participant had the highest number of touches of all participants, and also had the 3rd-lowest performance, so this participant was excluded from analysis. No other participants showed atypical task compliance, though 3/7 flagged participants had been excluded due to high participant-level FD or task-correlated motion as described above. The remaining 3/7 flagged participants did not show atypical task compliance by any objective metric and thus were retained in the sample.

2.6 *Performance Analysis*

Pen position was recorded at 60 Hz during drawing blocks of the fMRI task. To remove artifacts caused by the participant accidentally touching the tablet with a finger (which caused the recorded location to "jump" instantly across the tablet), raw data points were removed if their velocity (mm/sec) exceeded the 4th standard deviation, calculated within each scan. All analyses were performed in MATLAB 24.2.0 (Mathworks, Natick MA).

Based on the position data, six performance measures were calculated: position accuracy ("posErr" for brevity; -1 * position error, mm), smoothness "velSm" ("velSm;" -1 * number of velocity peaks per 45 mm shape part), direction accuracy "dirAcc" ("dirAcc;" -1 * direction error, degrees), velocity ("spd" to avoid confusion with velSm; root mean squared, mm / s), and two secondary measures: Balanced Integrated Score (BIS, "bis") and Speed Accuracy Tradeoff (SAT, "sat"), detailed in the following paragraphs.

BIS captures overall performance by integrating speed and accuracy measures (Liesefeld & Janczyk, 2023; Vandierendonck, 2021). BIS is calculated for each participant-hand pair (i.e. each participant had a LH and a RH value) as zscore(speed) + zscore(position accuracy), using participant-hand averages for speed and error, and z-scoring across the entire dataset (all participants & hands). An alternative calculation of BIS was explored using direction accuracy rather than position accuracy, but the two measures were highly correlated ($r^2 > 0.9$), so only position accuracy was used.

Table 3: Correlations between performance variables across hands.

	Coefficient of determination (r^2)		
Variable	**LH : RH**	**Asym : LH**	**Asym : RH**
Position Accuracy	0.357	0.038	0.427
Smoothness	0.829	0.009	0.228
Direction Accuracy	0.564	0.101	0.148
Velocity	0.856	0.003	0.101
SAT	0.865	0.000	0.112
BIS	0.826	0.036	0.048

SAT captures participant tradeoffs between fast (feedforward) and slow corrective (feedback) actions, to assess the participant's relative reliance on the two lateralized components in the complementary dominance hypothesis: the left-hemisphere feedforward specialization and right-hemisphere feedback specialization (Sainburg, 2002; Wang & Sainburg, 2007). Following our calculation of BIS, we determined SAT as zscore(speed) – zscore(position accuracy), such that a high SAT values will reflect a fast imprecise movement.

Performance variables were initially generated at the participant-hand level, but for each participant the LH and RH values were highly colinear, reflecting the existence of a "bilateral/overall dexterity" participant trait (**Table 3** column 1). To enable analysis of left/right performance differences without collinearity, an "asymmetry" value ("Asym") was calculated for each participant and variable as (RH-

LH)/(RH+LH) (after offset to minimum=0), such that high values represent the advantage of the preferred RH (Vingerhoets et al., 2023). Asymmetry's correlations with LH and RH were uniformly lower than the correlation between LH and RH, as shown in **Table 3** columns 2-3.

The "bilateral/overall dexterity" trait also manifested as across-variable correlations (**Supplementary Table 1**), which were addressed by avoiding collinearities via the 3-step model creation process described below (*ROI Analysis*).

Therefore, the final set of performance variables included 18 variables: six measures (position accuracy, smoothness, direction accuracy, velocity, BIS, SAT), each with separate values for LH, RH, and Asym.

2.7 *fMRI Analyses*

The task fMRI data were analyzed to identify where BOLD magnitude ("magnitude" for brevity) and/or FC were stronger for LH drawing than RH drawing ($hand_{LH-RH}$). In brief, data were reoriented into "ipsilateral/contralateral" (to movement) hemispheres, whole-brain magnitude was explored via a GLM analysis performed with FSL 6.0.7.12 (FMRIB, Oxford UK) (Smith et al., 2004), $hand_{LH-RH}$ effects on mangnitude were identified via a generalized linear mixed effects model (GLME) in each region of interest (ROI), and $hand_{LH-RH}$ modulation of FC was identified via generalized psychophysiological interaction (gPPI) (McLaren et al., 2012) performed with CONN 22.v2407 (Nieto-Castanon, 2020).

2.7.1 Data Reorientation: To allow direct comparison of LH vs. RH movement, the data from RH runs were left-right flipped after motion outlier identification and fMRIprep preprocessing, including registration to the symmetric template MNI152NLin2009cSym. This produced images where the left side of the image consistently represented the hemisphere ipsilateral to movement, and the right side the hemisphere contralateral to movement. Thereafter, all data were analyzed as "ipsilateral/contralateral" to movement.

2.7.2 Magnitude analysis (GLM): The reoriented data were integrated from fMRIprep to FSL using established workarounds (Mumford, 2017), followed by spatial smoothing with a 6 mm FWHM SUSAN filter and high pass temporal filtering with 60 sec cutoff; no other preprocessing was applied via FSL. Explanatory variables (EVs) were modeled, along with their temporal derivatives, according to the block design described in the previous section (*fMRI Task*), with additional confound EVs based on head motion parameters (3 variables each for translation and rotation) and motion outliers calculated as described above. The hemodynamic response was accounted for by convolving the model with a double-gamma function. Run-level contrasts of parameter estimates (COPEs) were calculated for Task vs. Rest. The run-level COPEs (Task > Rest) were averaged across runs using a fixed-effects model to produce participant-level results, which were used for subsequent analyses (the ROI analyses described in 2.7.3 and the whole-brain analyses described in the next paragraph).

Whole-brain analyses were performed to explore the data and identify additional areas with $hand_{LH-RH}$ effects to use as post hoc ROIs. Whole-brain analyses were performed using a mixed-effects model across participants (i.e. at the group level), including participant-specific EVs to capture the repeated-measures structure of LH vs. RH data within each participant, and one EV of interest. For the primary analysis of whole-brain magnitude data, the EV of interest was $hand_{LH-RH}$ (i.e. LH-RH differences within participants), coded as +1 for LH data and –1 for RH data. Secondary analyses were performed with alternate EVs of interest: (1) group, (2) $hand_{LH-RH}$ * group interaction, and (3) $hand_{LH-RH}$ * confound interaction, for each confound strong enough to be included in any of our ROI analysis models (see 2.7.4 *Magnitude ROI Analysis*, "model design" step). During all whole-brain analyses, Z-statistic images were created using cluster thresholding at $Z > 3.1$, $p < 0.05$.

In addition, the signal to noise ratio (SNR) was calculated for each participant as σ (Task>Rest) / σ (model), averaged across runs (Masharipov et al., 2024).

2.7.3 Region of Interest (ROI) selection: Twenty ROIs were used, 10 areas in each hemisphere (ipsilateral "-ipsi" and contralateral "-contra" to movement). These 20 included 12 *a priori* ROIs (preROIs) selected prior to data collection, and 8 post hoc ROIs (postROIs) selected using the whole-brain magnitude analysis. All ROIs were 4 mm radius spheres around a central seed voxel.

2.7.3.1 Selection of *A Priori* ROIs (preROIs): The 12 preROIs (6 areas * 2 hemisphres) were selected based on previous work implicating their roles in lateralized control of precision hand movement: M1, IPS, 7a, SPL, PMd, and SMA. The ROIs' seeds were determined from the following prior studies: The M1 seed was based on normative sensorimotor hand area (Philip & Frey, 2014; Smith & Frey, 2011). The IPS seed was chosen as the voxel with peak activation from left hemisphere areas that previously showed interhemispheric changes related to learning—specifically, where training-related increases in FC with right M1 correlated with NPH skill learning (Philip & Frey, 2016; fig. 4a). The 7a seed was chosen from the left hemisphere areas that previously showed interhemispheric changes related to learning and retention—specifically, where training-related changes in FC with right M1 predicted long-term retention of NPH skill (Philip & Frey, 2016; fig. 5a); for this ROI, the seed was selected as the first local maximum with >50% odds of being in cortex (which was also the local maximum with the greatest odds of being inside the brain, 78%) instead of the voxel of peak activation, because the peak was on the cortical surface (-34, -54, 67) and would have produced an ROI substantially outside the brain. The SPL seed was chosen as the voxel with peak activation from right hemisphere areas that previously showed convergent interhemispheric changes that predicted future learning—specifically, where pre-training FC from both left M1 and left IPS correlated with subsequent NPH learning (Philip et al., 2021; fig. 4). The PMd seed was chosen as the voxel with peak drawing-specific magnitude in left PMd (Philip et al., 2021; Potgieser et al., 2015). The SMA seed was chosen as the voxel with peak activation during a hand movement task that previously identified SMA as having a primary role in effective connectivity underpinning lateralized performance (Pool et al., 2014). Spheres were limited to the volume whose chance of being in the appropriate anatomical area according to the Juelich Histological Atlas (Eickhoff et al., 2006; Eickhoff et al., 2007) exceeded a cutoff; the cutoff for parietal and SMA ROIs was ≥ 25%, and PMd was ≥10% because its peak voxel only had a 21% chance of being in Brodmann's Area 6. However, these anatomical cutoffs did not lead to the removal of any voxels. When necessary, seeds from prior studies were transformed to the symmetric template MNI152NLin2009cSym (Fonov et al., 2009) via FLIRT before sphere creation. The ROI seed coordinates in the MNI152NLin2009cSym template were as follows: M1 (±40, −24, 56), IPS (±52, −42, 44), 7a (±20, −62, 68), SPL (±34, −58, 46), PMd (±26, −8, 52), and SMA (±6, −6, 56).

2.7.3.2 Selection of Post Hoc ROIs (postROIs): To identify areas with $hand_{LH-RH}$ effects outside our preROIs, 8 postROIs (4 areas * 2 hemispheres) were selected based on the significant clusters in the group-level analysis of $hand_{LH-RH}$ (see *2.7.2 Magnitude analysis*), using the following process. If a cluster overlapped with any preROI, the cluster was omitted. Each cluster was assigned to an anatomical area based on highest-weight assignment in the Harvard–Oxford cortical or subcortical atlas (Caviness Jr et al., 1996; Desikan et al., 2006; Seidman et al., 1999). If two clusters shared an assignment, correlation was assessed between the clusters' timecourses; and if significantly correlated, the lower-zscore cluster was omitted. For all remaining clusters, the center of gravity (and its homolog in the opposite hemisphere) was used as the seed for new bilateral postROIs. For a list of evaluated clusters, see *Results 3.1*. The final postROIs were as follows: inferior parietal lobule IPL (±52, -43, 30), primary somatosensory cortex S1 (±54, -21, 44), putamen (±27, -2, 5), and middle temporal gyrus MTG (±56, -54, -7).

2.7.4 Magnitude ROI Analysis: To identify factors that influenced BOLD magnitude in each ROI, a three-step process was performed for each ROI: univariate factor testing, model design, and a multivariable generalized linear mixed effects model (GLME). 22 candidate factors were used: 18 performance variables (6 measures * LH, RH, Asym; see *2.6 Performance Analysis*), age, sex (labeled "sexF" to indicate positive effects for female), group (patient, healthy), and drawing hand ("$hand_{LH-RH}$," i.e. LH-drawing > RH-drawing). $Hand_{LH-RH}$ was always included in the final GLME to address our study hypotheses, and therefore was ignored in factor testing and treated differently in model design.

In the first step (factor testing), a univariate t-score was produced for each candidate factor in each ROI. BOLD magnitude was modeled using a univariate general linear model (GLM), fit separately for each ROI based on each candidate factor (except for $hand_{LH-RH}$, which did not need testing because it was automatically included in the final model). This resulted in 420 univariate GLMs (20 ROIs * 21 factors).

In the second step (model design), a GLME model was built for each ROI using the most-relevant factors while avoiding collinearity. Specifically, the model for each area was built using the following process: Each area's model started with the factor "$hand_{LH-RH}$" to test the study hypothesis, and the random effect variable "subject" to address the repeated measures structure (2 values per participant, $hand_{LH}$ and $hand_{RH}$). Then, each other candidate factor was evaluated in order from highest to lowest absolute *T*-score (from factor testing): if the new factor was not correlated with any previously evaluated factors (Pearson's *r*, α = 0.05/# of tests), the new factor was added to the model. This process produced a model for each ROI with 7-9 factors: subject, hand, and 5-7 other candidate factors.

In the third step (multivariable GLME), BOLD magnitude in each ROI was modeled using a GLME via the MATLAB function 'fitglme,' with factors determined by the previous model design step. GLME was selected because BOLD magnitudes were normally distributed across participants. To assess statistical significance of each model vs. chance, the likelihood ratio test (MATLAB 'compare') was used. "Chance" was determined via a bootstrap method. In each draw, factor values were randomly permuted across participants, independently for each factor; and a p-value was calculated using the likelihood ratio test. Reported p-values represent the average across 500 draws. To assess statistical significance of individual factors, multiple comparisons were controlled via Benjamini–Hochberg false discovery rate (FDR) (Benjamini & Hochberg, 1995) across the 20 GLMEs, with significance set at FDR-corrected $p < 0.05$, separately for $hand_{LH-RH}$ (primary analysis) and other factors (exploratory).

In the cases where postROI GLME analyses were statistically invalid due to double-dipping (i.e. selecting and analyzing ROI from the same data; Kriegeskorte et al., 2009), p-values were not reported, though T-scores were still reported to enable comparison between ROIs. In these cases, interpretations were based on the original selective analysis (whole-brain magnitude analysis, *2.7.2*).

In addition to the above analyses of $hand_{LH-RH}$ effects, the effect size of Group (patient vs. healthy adult) on BOLD magnitude was calculated for each ROI as Cohen's *d* via the MATLAB 'meanEffectSize' function.

2.7.5 Functional Connectivity (FC) & Generalized Psychophysiological Interaction (gPPI) analysis: To idenfify hand-dependent ($hand_{LH-RH}$) modulation of FC, a gPPI analysis was performed in the CONN toolbox (22.v2407). First, the reoriented data were smoothed using spatial convolution with a Gaussian kernel of 6 mm FWHM; no other preprocessing was applied via CONN. Denoising was performed using the standard CONN pipeline (Nieto-Castanon, 2020), which included regressing out confounding signals from white matter and CSF BOLD signals (five components each), based on the anatomical component-based noise correction method (aCompCor) (Behzadi et al., 2007) along with six realignment parameters

and their first derivatives, outlier scans, condition effects and their first-order derivatives, and linear detrending. High-pass filtering was subsequently applied to retain signal fluctuations above 0.008 Hz.

ROI-to-ROI functional connectivity modulation ($hand_{LH-RH}$) between the twelve preROIs was evaluated via gPPI. For each seed–target ROI pair, the subject-level model included three predictors: (i) HRF-convolved psychological regressors for condition (drawRH, drawLH, and rest); (ii) the physiological regressor (the seed ROI BOLD time series); and (iii) condition-specific interaction terms (PPI) formed by multiplying (i) and (ii), indexing modulation of connectivity between the ROIs. For each connection, the condition-dependent modulation was quantified as the bivariate regression coefficient (β) for the PPI (i.e. interaction) term. At the group level, these PPI β values were analyzed with connection-wise random-effects GLMs across participants to test task effects; the primary contrast was drawLH > drawRH (i.e. $hand_{LH-RH}$). Multiple comparisons were controlled using CONN's parametric, connection-based framework with Benjamini–Hochberg false discovery rate (FDR) across connections; significance was set at FDR-corrected $p < 0.05$.

To contextualize gPPI's connectivity-modulation values with a measurement of actual connectivity, standard ROI-to-ROI FC (not gPPI) was estimated separately for LH > rest and RH > rest (e.g. Agren & Hoppe, 2024).

In addition to the above analyses of $hand_{LH-RH}$ modulation, the influence of group (patient vs. healthy adult) on gPPI was assessed by examining effects of group and the group*$hand_{LH-RH}$ interaction.

3. RESULTS

We found that, during LH execution of a visually guided precision drawing task (vs. RH), M1 contralateral to movement showed lower BOLD magnitude, and greater functional connectivity (FC) with two networks: M1/PMd ipsilateral to movement, and parieto-temporal areas contralateral to movement, both of which had equal-or-greater magnitude. During RH execution, M1 contralateral to movement showed greater connectivity with IPL ipsilateral to movement, which had greater BOLD magnitude.

3.1 *Exploratory whole-brain analysis reveals LH-specific BOLD signal in sensorimotor and parieto-temporal areas*

To explore effects of drawing hand on BOLD magnitude across the brain, we performed an exploratory whole-brain group-level analysis of $hand_{LH-RH}$. These whole-brain results (**Figure 2**) included 7 clusters, divided between sensorimotor regions ipsilateral to movement (M1, SMA, S1, putamen) and parieto-temporal regions contralateral to movement (MTG and IPL), as detailed in **Table 4**.

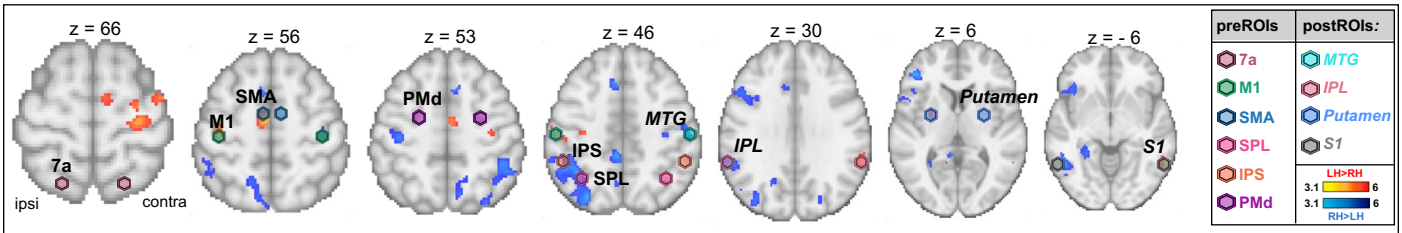

Figure 2: Whole-brain analysis of $hand_{LH-RH}$ effects, overlaid with all ROIs for comparison. 7 significant clusters were found, of which 4 were unique and used as seeds for 8 bilateral postROIs (italicized; see Table 4). "Ipsi" = ipsilateral to drawing hand, "contra" = contralateral to drawing hand.

Comparing the exploratory whole-brain results with our preROIs, the 2 strongest clusters overlapped our preROIs in M1-ipsi and SMA-ipsi, while the other 5 clusters were outside our preROI. To expand our set of ROIs for subsequent analyses, we first reduced the 5 novel clusters to 4 unique clusters (two redundant clusters in IPL, timecourse correlation $r = 0.812$, $p < 0.001$), and used those 4 unique cluster peaks as seeds for 8 bilateral post hoc ROIs (postROIs) used in all subsequent analyses.

Table 4: Significant clusters in whole-brain contrast LH>RH ($hand_{LH-RH}$) of BOLD magnitude.

Cluster Index	Voxels	p	Z-MAX	Z-COG X (mm)	Z-COG Y (mm)	Z-COG Z (mm)	Anatomical region	Used to create post hoc ROI?
7	421	<0.001	4.85	-30.2	-17.8	66.1	M1 (ipsi)	No[1]
6	204	0.001	5.36	-6.92	-9.57	59	SMA (ipsi)	No[1]
5	136	0.013	5.46	61.6	-43.3	30.5	IPL (contra)	Yes[2]
4	125	0.019	4.76	-54	-21.1	44.4	S1 (ipsi)	Yes
3	121	0.021	4.21	-26.7	-2.06	5.28	Putamen (ipsi)	Yes
2	99	0.047	4.35	55.7	-54.2	-6.95	MTG (contra)	Yes
1	98	0.049	3.8	53.7	-54.1	39.1	IPL (contra)	No[2]

Notes: Significance determined at cluster-corrected $p < 0.05$. [1]: Overlapped with the preROI in the same region. [2]: Clusters #2 and #5 were correlated, so only #2 was used.

In addition, we performed another whole-brain group-level analysis to assess the effect of confounds on our $hand_{LH-RH}$ results. Only one confound factor, sexF, was strong enough for inclusion in any of our ROI analyses (see next section) and thus tested here. A whole-brain analysis of the of the $hand_{LH-RH}$ * sexF interaction revealed no significant clusters, indicating that our $hand_{LH-RH}$ results were not affected by confounds.

3.2 *Drawing with the LH involves higher BOLD magnitude in ipsilateral frontal motor and contralateral parietal regions of interest*

For our primary analysis, we tested whether BOLD magnitude varied with drawing hand (i.e. $hand_{LH-RH}$) in our ROIs. 20 ROIs were used: 10 areas * 2 hemispheres, ipsilateral and contralateral to movement, which including all 12 preROIs and 8 postROIs. In each ROI we modeled BOLD signal magnitude with a GLME that included $hand_{LH-RH}$ and the strongest non-collinear performance/confound factors (for factor strengths see **Supplementary Tables 2-3**).

Multiple bilateral cortical areas were sensitive to $hand_{LH-RH}$, with significant effects in 13/20 ROIs as visualized and quantified in **Figure 3.** For full model details, see **Supplementary Tables 4-5**. Each of the 13 ROIs fell into one of two response categories. In the first category, sensorimotor and frontal motor areas (M1, S1, SMA, putamen) showed a positive effect of $hand_{LH-RH}$ in the ipsilateral hemisphere, paired with a negative $hand_{LH-RH}$ effect in the contralateral hemisphere that reached significance in 2/4 ROIs (M1, S1). In the second category, parietal and temporal areas (SPL,IPS, IPL, MTG) showed the reverse pattern, with a negative effect of $hand_{LH-RH}$ (RH > LH) in the ipsilateral hemisphere, paired with a positive effect (LH > RH) in the contralateral hemisphere that reached significance in 3/4 ROIs (IPS, IPL, MTG). In other words, drawing with the LH (vs. RH) led to greater ipsilateral BOLD magnitude in motor/subcortical areas, but greater contralateral BOLD magnitude in parieto-temporal areas.

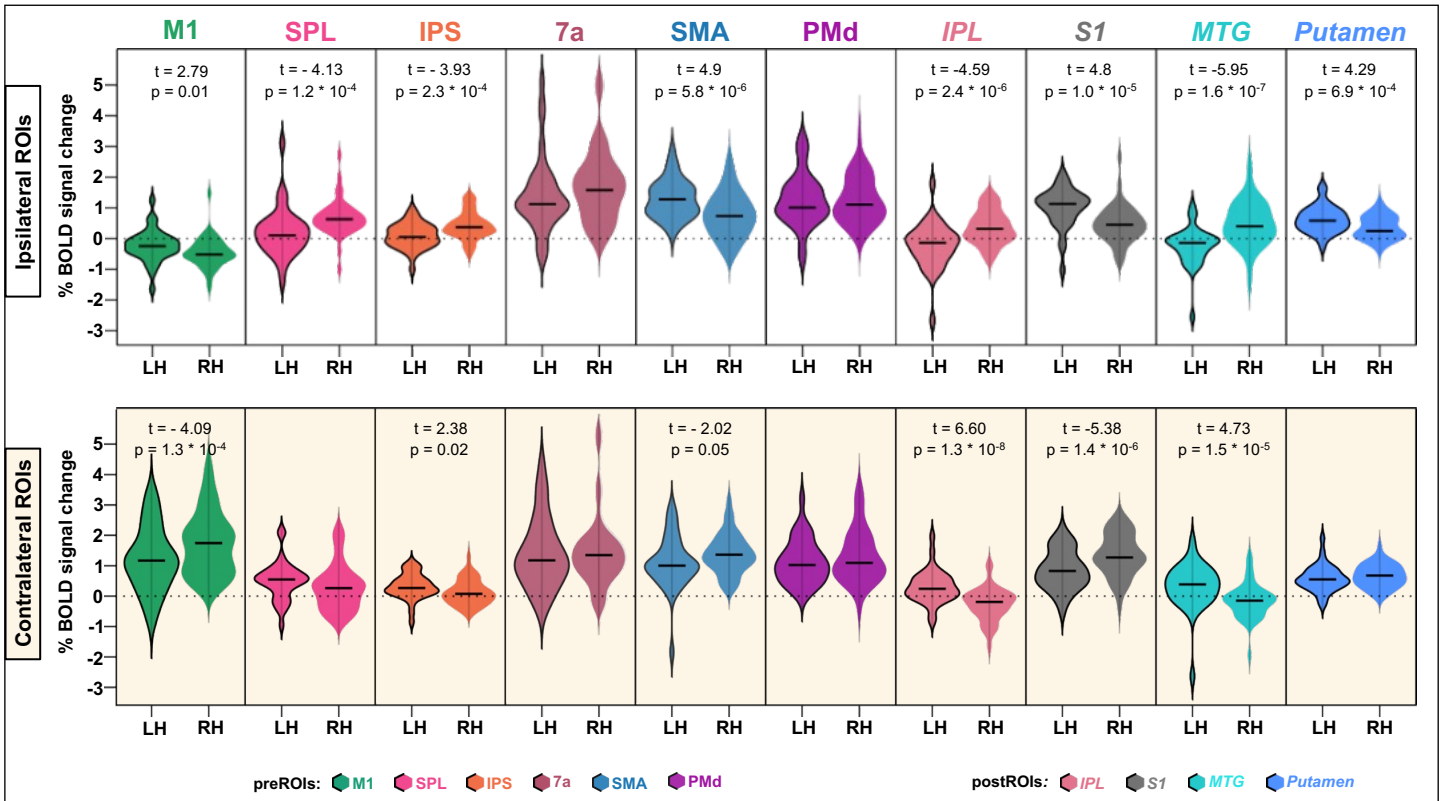

Figure 3: Hand$_{LH-RH}$ effects on BOLD magnitude in pre- and post-ROIs. The effect of hand$_{LH-RH}$ in M1/SMA and S1/Putamen is ipsilateral +, contralateral –; whereas in SPL/IPS and IPL/MTG, the effect is ipsilateral –, contralateral +. Statistics from GLME.

Performance-related effects did not achieve statistical significance in any ROI after multiple comparison correction ($p > 0.07$), as expected because the current design was powered to detect effects of the factor hand$_{LH-RH}$, not quantitative effects of performance.

To quantify data quality, we evaluated the SNR of the task effect (Draw > Rest) on BOLD magnitude. Our study achieved SNR 0.487 ± 0.08.

3.3 *Functional connectivity: LH drawing depends on bilateral parieto-motor interactions*

We evaluated hand-specific modulation of FC between the 20 ROIs via a gPPI analysis, which revealed siginificant hand$_{LH-RH}$ modulation in 26 connections between 16/20 ROIs, as shown in **Supplementary Figure 1**. To constrain the influence of postROI over preROI (i.e. of post-hoc analyses over *a priori*), we did not interpret connections involving preROIs that had no significant FC modulation in a preROI-only analysis (**Supplementary Table 6**). Following this constraint, we interpreted hand$_{LH-RH}$ FC modulation in 11 connections involving 10/20 ROIs, as shown in **Figure 4** and listed in **Table 5**.

To contextualize this hand-dependent modulation, we examined traditional FC (not gPPI modulation) between ROIs, separately for each drawing condition (LH, RH). All five connections identified by gPPI had FC > 0 in both conditions, with numerically stronger FC during LH (t-score range 3.07–12.64, FDR-corrected $p < .001$) than RH (t-score range 2.16–7.92, FDR-corrected $p \leq .015$). This indicates that the positive gPPI modulation for hand$_{LH-RH}$ reflects a strengthening of pre-existing positive connectivity.

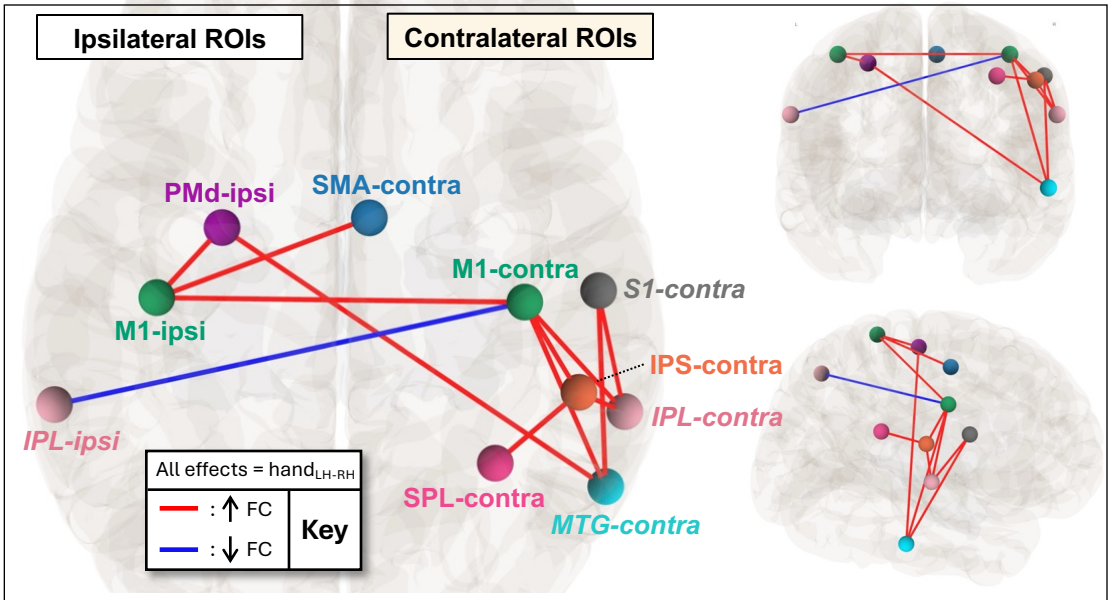

Figure 4: gPPI modulation of functional connectivity (FC) for hand$_{LH-RH}$, after constraining interpretation to prevent post-hoc analyses from altering *a priori* analyses. Under this constraint, 11 connections between 10/20 ROIs showed significant gPPI modulation.

Table 5: Functional connections with significant hand$_{LH-RH}$ modulation

ROI 1	ROI 2	T-score	p-value
IPL-contra	*S1-contra*	4.69	0.0061
PMd-ipsi	M1-ipsi	4.37	0.0160
M1-contra	M1-ipsi	4	0.0230
M1-contra	*MTG-contra*	3.91	0.0192
IPS-contra	SPL-contra	3.8	0.0272
M1-contra	*IPL-ipsi*	-3.71	0.0247
S1-contra	*MTG-contra*	3.52	0.0307
M1-contra	IPS-contra	3.5	0.0453
M1-ipsi	SMA-contra	3.41	0.0470
PMd-ipsi	*MTG-contra*	3.28	0.0432
M1-contra	IPL-contra	3.25	0.0451

Note: *P*-values corrected for false discovery rate. Italics = post hoc ROI.

3.4 *Magnitude-connectivity integration: during LH drawing, right M1 decreases magnitude but increases connectivity with left motor-premotor and right parietal-occipital areas.*

To integrate our fMRI analyses, we visualize our BOLD magnitude and FC modulation effects together in **Figure 5**. Together, these results show that the hand$_{LH-RH}$ effect involved the corticospinal output area M1-contra reducing magnitude but increasing connectivity. Specifically, for hand$_{LH-RH}$ drawing, M1-contra had stronger interhemispheric FC with M1-ipsi, which had higher magnitude and stronger FC with PMd-ipsi and SMA-contra. At the same time, M1-contra also had stronger intrahemisphereric FC with contralateral parieto-temporal regions that mostly have higher magnitude (IPL, MTG, IPS, but not SPL). We also found

that S1-contra followed the same pattern as M1-contra: lower magnitude, but increased FC with higher-magnitude areas (here, IPL-contra and MTG-contra). Finally, IPL-ipsi had a distinct hand$_{LH-RH}$ effect, with lower magnitude and weaker interhemispheric FC with M1-contra.

Overall, by combining BOLD magnitude and FC modulation, our results indicate that, during LH precision drawing, motor output (i.e. M1-contra) is primarily connected with ipsilateral left motor-premotor and contralateral right parieto-temporal areas, but disconnected from ipsilateral left inferior parietal cortex.

3.5 Patients with peripheral nerve injury show the same hand-specific effects as healthy adults

To address our hypothesis that patients with chronic PNI would use the same neural mechanisms as healthy adults for LH drawing, we first evaluated whether Group (patient vs. healthy) contributed to any GLME of BOLD magnitude. Group did not contribute significantly to any GLME model (|T-score|

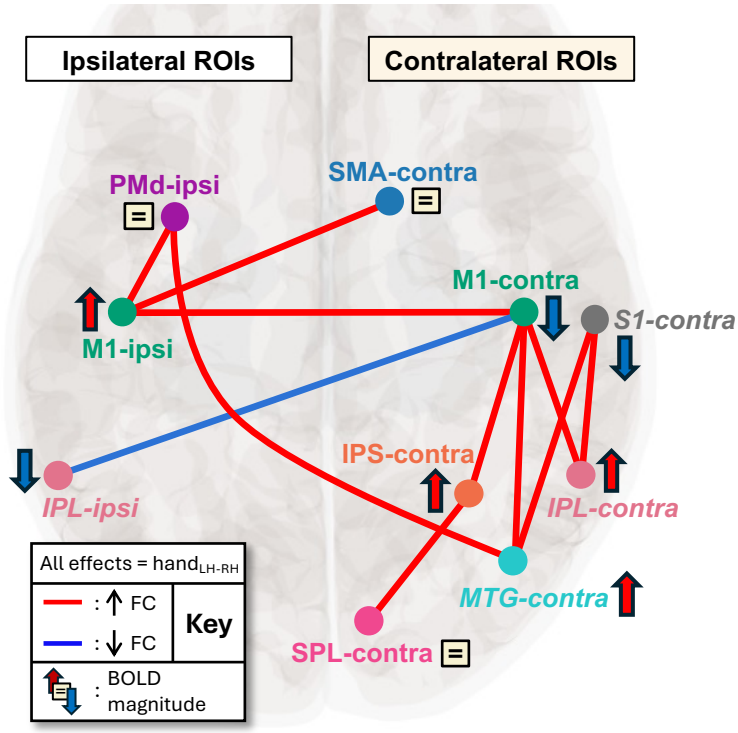

Figure 5: Integrated visualization of BOLD magnitude and functional connectivity (FC) modulation for hand$_{LH-RH}$, across ROIs. ROIs are shown if any of their connections had significant gPPI modulation (lines); if shown, BOLD magnitude differences (arrows) are overlaid.

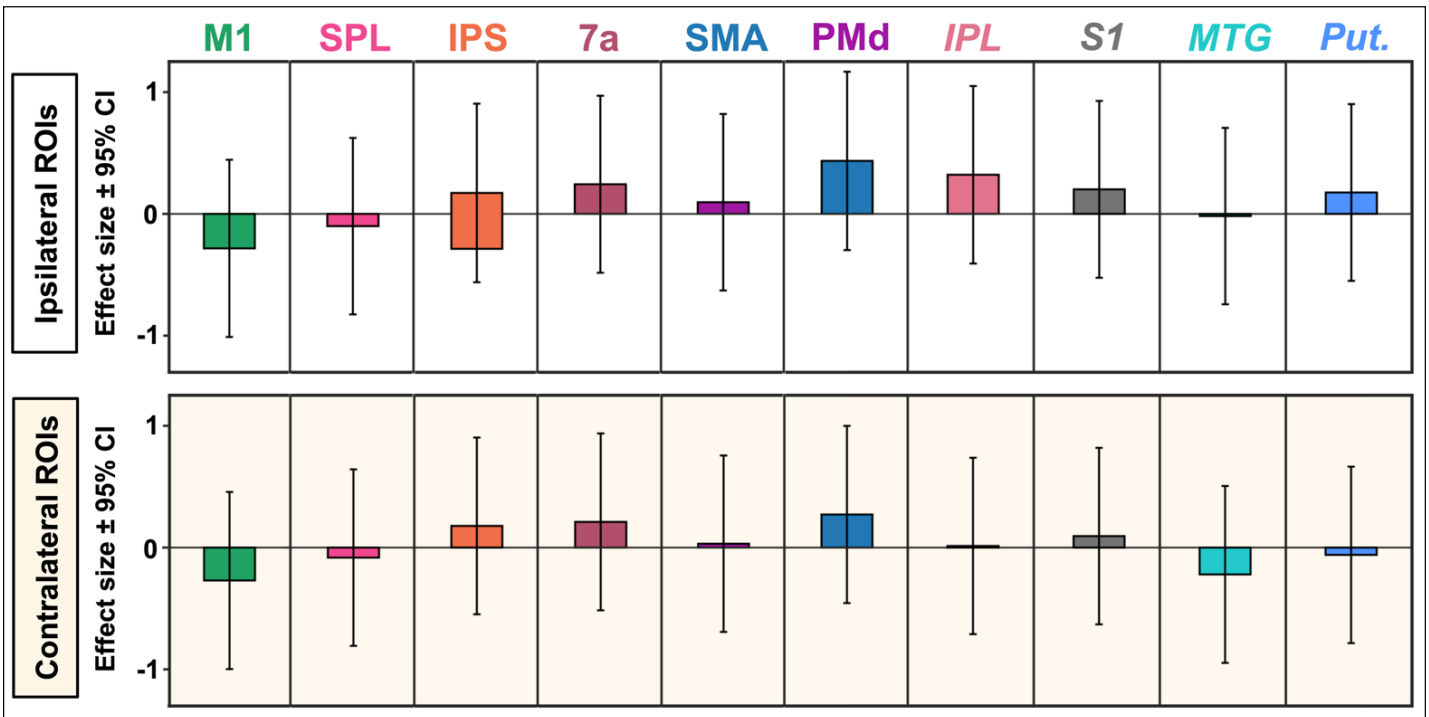

Figure 6: No effect of group (healthy adult vs. peripheral nerve injury patient) on BOLD magnitude. In every ROI, 95% confidence intervals of effect size (Cohen's d) include zero. Put. = putamen.

range 0.66-1.55, p-uncorrected ≥ 0.15; **Supplementary Table 4**). To confirm this negative result, we evaluated the univariate effect size of Group in each ROI, and found that its 95% confidence interval included zero in all ROIs, whether combining data from LH and RH drawing ($p > 0.08$, **Figure 6**) or separately analyzing LH and RH ($p > 0.22$).

Group also had no effect on any other fMRI measure. Whole-brain BOLD magnitude analysis revealed no significant clusters for Patient > Healthy, Healthy > Patient, nor for the interactions Group*$Hand_{LH-RH}$ or Group*SexF. gPPI analysis revealed no connections with significant gPPI modulation (positive or negative) with Group or Group*$Hand_{LH-RH}$. Therefore, we found no evidence that any of our $hand_{LH-RH}$ effects differed between patients and healthy adults.

4. DISCUSSION

Our study used a visually-guided precision drawing task to characterize neural activity and functional connectivity associated with left hand (LH) drawing in right-handed individuals, with and without unilateral right hand (RH) peripheral nerve injury (PNI). We identified two mechanisms that supported LH precision drawing, and one specific to RH precision drawing, as shown in **Figure 7**. Overall, control of the non-preferred LH relied on a combination of interhemispheric and intrahemispheric processes: motor output (right M1) was supported by adapting a dominant (left) hemisphere motor-premotor network via enhanced interhemispheric integration, and increasing intrahemispheric engagement of secondary motor areas in the contralateral hemisphere. In contrast, RH drawing was associated with increased engagement of an interhemispheric M1–IPL network typically recruited during tool use. The performance differences between the LH and RH may therefore be explained by right M1's indirect connections to the left motor-premotor network, and its incomplete access to a parietal-motor network for tool use. These neural mechanisms did not differ between healthy ad ults and patients with chronic RH PNI.

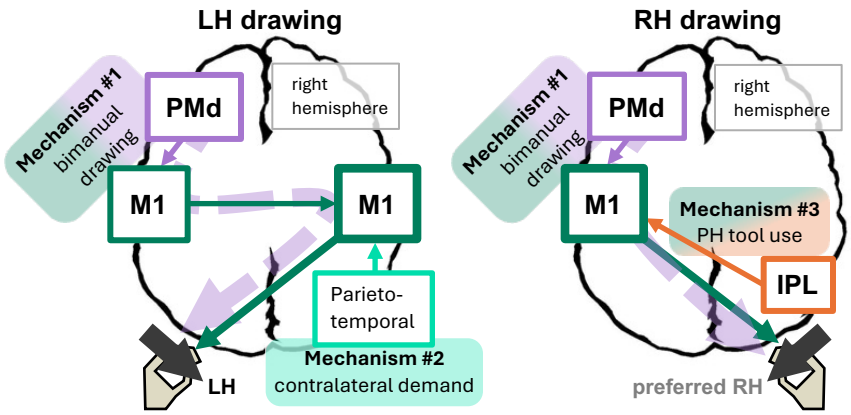

Figure 7: Model of neural mechanisms with differential involvement in left hand (LH) vs. right hand (RH) precision drawing, in right-handed adults. **Mechanism #1** is a left M1-PMd network for bimanual drawing, with access to contralateral M1 via hand-specific paths (dashed lines): an indirect interhemispheric path during LH drawing, and a direct intrahemispheric path during RH drawing. **Mechanism #2** is an intrahemispheric parieto-temporal network for LH drawing, potentially representing increased engagement of contralateral visuomotor networks to support the high demands action of LH action. **Mechanism #3** is an interhemispheric M1-IPL network for RH drawing, potentially reflecting a unique lateralization for tool use and praxis with the preferred hand (PH).

4.1 *Left-hemisphere motor-premotor network supports bimanual precision drawing*

We found a left-lateralized M1-PMd network that functions as a shared neural mechanism for bimanual precision drawing in right-handed adults. This is our primary finding because it is the only mechanism entirely composed of preROIs. This network may involve M1's role in ipsilateral motor control under

complex or high-demand conditions (Barany et al., 2020; Buetefisch et al., 2014; Kim et al., 1993; Verstynen et al., 2005) and left PMd's role in the temporal aspects of bilateral movement and their associated task-specific demands (Kornysheva & Diedrichsen, 2014; Schluter et al., 1998; Yang et al., 2024). During RH drawing, this network includes contralateral left M1 as the source of descending corticospinal control output. During LH drawing, contralateral (right) M1 is not part of the network; instead, descending control is supported via interhemispheric connectivity from the network to contralateral M1. Thus, the left-lateralized M1-PMd network retains its role across hands by adaptively recruiting contralateral motor regions via interhemispheric M1-M1 connections (**Figure 7**, Mechanism #1).

This left-lateralized M1-PMd network provides anatomical specificity to existing models of hand dominance, which propose that RH advantages in right-handed individuals arise from a left hemisphere specialization for predictive dynamics that enable precise movement (complementary dominance), and LH disadvantages for precise movement arise from interhemispheric delays (Kitchen et al., 2025; Liepmann, 1905; B. A. Shabbott & R. L. Sainburg, 2008). It is also consistent with previous findings that FC in a M1-PMd-somatosensory network supports precision manual tasks with the RH (Yang et al., 2024). Here we extend this work by specifying this left-lateralized mechanism and demonstrating its hand-specific connection to cortical outputs: direct intrahemispheric during RH drawing, and indirect interhemispheric during LH drawing.

Our effector-independent role for left PMd diverges from the findings of Potgieser et al. (2015), who reported bilateral PMd activation during a visually guided figure-copying task. This difference may depend on task characteristics: unlike Potgieser et al. (2015), our task imposed constrains on spatial precision, which affects lateralization across parietal and premotor cortices (Haaland et al., 2004).

4.2 *Right parieto-temporal network supports the execution of demanding tasks with the left hand.* We identified a parieto-temporal network (SPL, IPS, IPL, MTG) that became more engaged with right M1 for $\text{hand}_{\text{LH-RH}}$. This network had greater intrahemispheric (right hemisphere) connectivity with right M1 alongside increased activity in most of the network (IPL, IPS, MTG) but not all (SPL). Right posterior parietal areas are involved in various aspects of visuomotor control: goal-directed visuospatial attention (Corbetta et al., 2000; Wang et al., 2016), combining and maintaining representations of goal and movement (Averbeck et al., 2009; Wolpert et al., 1998), motor skill learning (Della-Maggiore et al., 2004), and action planning with the contralateral hand (Valyear & Frey, 2015); and the roles of right MTG include monitoring intersensory conflict (van Kemenade et al., 2019) and the visual evaluation of action quality (Jastorff et al., 2010). This network is unlikely to represent the right hemisphere's specializations for impedence components of movement (Kitchen et al., 2025), because such a specalization should show increased interhemispheric connectivity during RH drawing (when a right hemisphere mechanism supports left M1). Therefore, we propose that the right parieto-temporal network represents a broad contralateral-hemisphere visuomotor control network that becomes more engaged during LH drawing due to the increased task demands of in drawing with the NPH (**Figure 7**, Mechanism #2).

4.3 *Interhemispheric parietal-motor network supports tool use and praxis with the right hand.* We found differential $\text{hand}_{\text{LH-RH}}$ disengagement of ipsilateral IPL: it had lower activity, and its interhemispheric IPL-M1 connection was the only connection with negative modulation for $\text{hand}_{\text{LH-RH}}$ (which can also be represented as positive modulation for $\text{hand}_{\text{RH-LH}}$). This unique disengagement suggests a mechanism that supports drawing with the preferred RH but (unlike Mechanism #1) is not effectively adapted to support LH drawing. IPL is involved in sensorimotor integration for praxis and tool use, though it remains unclear whether those functions are lateralized to left IPL (Buxbaum et al., 2007;

Rosenzopf et al., 2022; Wheaton et al., 2009) or right IPL (Ras et al., 2022; Singh-Curry & Husain, 2009). This tool use function is consistent with our choice of task, which involved a tool with high sensorimotor control demands (drawing with a stylus, in an unfamiliar position, viewed with a mirror). Therefore, we propose that the interhemispheric IPL–M1 network represents a mechanism for tool use with the preferred hand (**Figure 7**, Mechanism #3).

This tool use network is likely independent from Mechanism #1's left hemisphere specialization for bimanual precision (i.e. complementary dominance). Tool use and complementary dominance may have separate evolutionary origins (Sainburg, 2014; Uomini, 2009; Uomini & Ruck, 2018; Versace & Vallortigara, 2015), and the neural mechanisms for tool use seem to be lateralized to the left hemisphere regardless of hand preference or dominance (Frey et al., 2005), though most neuroimaging evidence comes from pantomime (Vingerhoets et al., 2012) or action observation paradigms (Haberling et al., 2016). Our findings extend this literature by demonstrating distinct and potentially separable neural mechanisms for tool use and precision control.

4.4 *Patients with peripheral nerve injury control their non-preferred left hand via the same mechanisms as healthy adults*

Participants with chronic RH PNI recruited the same three mechanisms as healthy controls, implying that all three mechanisms remain intact and accessible after chronic unilateral PNI. Its engagement during LH drawing in patients carries promising clinical implications, as it provides a target for neuromodulatory or behavioral interventions aimed at improving NPH function. Multiple rehabilitation approaches have demonstrated efficacy in enhancing NPH performance, including bimanual training (Stinear & Byblow, 2004), mirror therapy (Dohle et al., 2009; Nojima et al., 2012), action observation (Ertelt et al., 2007), motor imagery (Sharma et al., 2006), and bihemispheric stimulation strategies such as dual tDCS or rTMS (Lindenberg et al., 2010; Waters-Metenier et al., 2014). These approaches converge on the principle that bilateral cortical recruitment, particularly via the dominant hemisphere, can facilitate motor recovery or compensation after unilateral impairment.

In addition, this work helps establish a normative template of bilateral cortical control for precision movement in the healthy brain. Such a template is critical for rehabilitation of asymmetric neurological conditions such as stroke, wherein some patients must rely on their NPH due to chronic PH impairment. For example, researchers and clinicians can now determine whether a patient is using their NPH with a typical brain mechanism (i.e. the left M1-PMd network) versus an atypical brain mechanism, or whether reduced interhemispheric connectivity might impede the typical mechanism. This will allow researchers to characterize atypical mechanisms, and may allow clinicians to predict which patients can learn to effectively use their NPH. Overall, our study provides the essential groundwork to identify atypical and pathological neural mechanisms, and ultimately to design individualized, mechanism-driven rehabilitation protocols that improve outcomes and restore function across a range of unilateral motor impairments.

4.5 *Ipsilateral superior parietal lobule may be learning-dependent*

Our results did not support our initial hypothesis that a locus in ipsilateral SPL would play a greater role during LH than RH drawing. SPL did show recruitment for LH drawing (increased FC, effector-independent activity), but in contralateral rather than ipsilateral SPL; in other words, right SPL is more connected to M1 motor output during LH drawing, than left SPL is for RH drawing. We interpret this as part of a contralateral task demand network (4.2, Mechanism #2). We based our initial hypothesis on previous findings that interhemispheric FC involving ipsilateral left SPL could predict future LH skill learning (Philip et al., 2021). However, the current study did not involve learning: participants completed

only 5.5 minutes of familiarization with each hand, followed by 16.5 minutes with each hand during fMRI, far below the amount of time required for right-handed adults to learn a LH precision drawing task (4.6 ± 2.3 sessions of 20 minutes each; Philip & Frey, 2016). Therefore, our SPL locus may capture an ipsilateral mechanism specific to LH skill learning.

5. *Limitations*

This study had a relatively modest sample size (n = 33). However, this sample size was appropriate for detecting our primary task-related activation effects (i.e., $hand_{LH-RH}$ contrasts), as determined by our *a priori* power analysis. Further supporting our modest sample size, our drawing movement task produced larger neurological effects the designs used to create most sample size benchmarks, as demonstrated by our SNR of 0.49, approaching the 0.5 practical upper limit for task fMRI (Masharipov et al., 2024). Nevertheless, we adapted our analysis to our modest sample size by declining to evaluate the quantitative brain-behavior relationships that are most likely to produce unstable results at small sample sizes (Grady et al., 2020), and treating gPPI as a secondary analysis because simulation studies suggest n ≥ 50 to detect gPPI effects in a block design study of SNR ~0.5 (Masharipov et al., 2024). For quantitative analyses (e.g. performance) and robust gPPI results, further studies with larger sample sizes are necessary [link to pre-registration will be added after peer review].

Our current analysis confounds hand and task demands (i.e. because LH movements are more difficult). Due to this limitation we present our interpretation of Mechanism #2 (contralateral task demand) as a hypothesis, which will be tested in future studies that independently manipulate hand and task demands.

Our results describe neural mechanisms specific to the control of precision drawing (a PH-specialized task) in right-handed adults. Therefore, our findings provide no information about neural mechanisms of NPH specializations, nor about left-handed individuals.

6. *Conclusion*

This study identified three neural mechanisms that distinguish LH vs. RH drawing in right-handed adults. First, a left-lateralized M1-PMd network for bilateral precision control, which is engaged interhemispherically during LH drawing and intrahemispherically during RH drawing, and may represent complementary dominance. Second, a contralateral parieto-temporal network for visuomotor integration, which is more engaged during LH drawing, potentially due to its high task demands. Third, an interhemispheric parietal-motor network, potentially for tool use, is more engaged during RH drawing. In addition, individuals with chronic PNI to their right hand used the same neural mechanisms, indicating that cortical adaptation after injury may leverage pre-existing dominant-hemisphere and interhemispheric networks.

These findings provide a specific neuroanatomical basis for existing theories of handedness, including a potential neural mechanism for observed behavioral asymmetries in upper limb performance. The left M1–PMd network's role in bilateral control highlights it as a compelling target for neuromodulatory and rehabilitative interventions to enhance motor function after injury.

ACKNOWLEDGEMENTS

The authors would like to thank Summer Fletcher for their help with data collection and logistics, and Joshua Shimony for his help with patient safety. This study was funded by NIH/NINDS grant R01NS114046 to BAP. Data storage was funded by NCI grant P30 CA091842 and NCATS grant UL1 TR002345 to Washington University.

References

Abraham, A., Pedregosa, F., Eickenberg, M., Gervais, P., Mueller, A., Kossaifi, J., Gramfort, A., Thirion, B., & Varoquaux, G. (2014). Machine learning for neuroimaging with scikit-learn. *Frontiers in neuroinformatics*, *8*, 14.

Agren, T., & Hoppe, J. M. (2024). Extensive functional connectivity between brain areas implicated in mental imagery production and phobic fear during both emotional and neutral mental imagery. *Behav Brain Res*, *462*, 114893. https://doi.org/10.1016/j.bbr.2024.114893

Avants, B. B., Epstein, C. L., Grossman, M., & Gee, J. C. (2008). Symmetric diffeomorphic image registration with cross-correlation: evaluating automated labeling of elderly and neurodegenerative brain. *Medical image analysis*, *12*(1), 26-41.

Averbeck, B. B., Crowe, D. A., Chafee, M. V., & Georgopoulos, A. P. (2009). Differential contribution of superior parietal and dorsal-lateral prefrontal cortices in copying. *Cortex*, *45*(3), 432-441. https://doi.org/10.1016/j.cortex.2008.02.007

Barany, D. A., Revill, K. P., Caliban, A., Vernon, I., Shukla, A., Sathian, K., & Buetefisch, C. M. (2020). Primary motor cortical activity during unimanual movements with increasing demand on precision. *Journal of Neurophysiology*, *124*(3), 728-739.

Beaton, D. E., Davis, A. M., Hudak, P., & McConnell, S. (2001). The DASH (Disabilities of the Arm, Shoulder and Hand) outcome measure: what do we know about it now? *The British Journal of Hand Therapy*, *6*(4), 109-118.

Behzadi, Y., Restom, K., Liau, J., & Liu, T. T. (2007). A component based noise correction method (CompCor) for BOLD and perfusion based fMRI. *NeuroImage*, *37*(1), 90-101. https://doi.org/10.1016/j.neuroimage.2007.04.042

Benjamini, Y., & Hochberg, Y. (1995). Controlling the false discovery rate: a practical and powerful approach to multiple testing. *Journal of the Royal statistical society: series B (Methodological)*, *57*(1), 289-300.

Blank, R., Miller, V., & Von Voss, H. (2000). Human motor development and hand laterality: a kinematic analysis of drawing movements. *Neuroscience Letters*, *295*(3), 89-92.

Bottenhorn, K. L., Flannery, J. S., Boeving, E. R., Riedel, M. C., Eickhoff, S. B., Sutherland, M. T., & Laird, A. R. (2018). Cooperating yet distinct brain networks engaged during naturalistic paradigms: A meta-analysis of functional MRI results. *Network Neuroscience*, *3*(1), 27-48. https://doi.org/10.1162/netn_a_00050

Buetefisch, C. M., Revill, K. P., Shuster, L., Hines, B., & Parsons, M. (2014). Motor demand-dependent activation of ipsilateral motor cortex. *Journal of Neurophysiology*, *112*(4), 999-1009. https://doi.org/10.1152/jn.00110.2014

Buxbaum, L. J., Kyle, K., Grossman, M., & Coslett, B. (2007). Left inferior parietal representations for skilled hand-object interactions: evidence from stroke and corticobasal degeneration. *Cortex*, *43*(3), 411-423.

Caviness Jr, V. S., Meyer, J., Makris, N., & Kennedy, D. N. (1996). MRI-based topographic parcellation of human neocortex: an anatomically specified method with estimate of reliability. *Journal of Cognitive Neuroscience*, *8*(6), 566-587.

Corbetta, M., Kincade, J. M., Ollinger, J. M., McAvoy, M. P., & Shulman, G. L. (2000). Voluntary orienting is dissociated from target detection in human posterior parietal cortex. *Nature neuroscience*, *3*(3), 292-297.

Dale, A. M., Fischl, B., & Sereno, M. I. (1999). Cortical surface-based analysis: I. Segmentation and surface reconstruction. *NeuroImage*, *9*(2), 179-194.

Della-Maggiore, V., Malfait, N., Ostry, D. J., & Paus, T. (2004). Stimulation of the posterior parietal cortex interferes with arm trajectory adjustments during the learning of new dynamics. *The Journal of*

Neuroscience: the Official Journal of the Society for Neuroscience, *24*(44), 9971-9976. https://doi.org/10.1523/JNEUROSCI.2833-04.2004

Desikan, R. S., Segonne, F., Fischl, B., Quinn, B. T., Dickerson, B. C., Blacker, D., Buckner, R. L., Dale, A. M., Maguire, R. P., Hyman, B. T., Albert, M. S., & Killiany, R. J. (2006). An automated labeling system for subdividing the human cerebral cortex on MRI scans into gyral based regions of interest. *NeuroImage*, *31*(3), 968-980. https://doi.org/10.1016/j.neuroimage.2006.01.021

Dexheimer, B., Sainburg, R. L., Sharp, S., & Philip, B. A. (2024). Roles of Handedness and Hemispheric Lateralization: Implications for Rehabilitation of the Central and Peripheral Nervous Systems: A Rapid Review. *American Journal of Occupational Therapy*, *78*(2). https://doi.org/10.5014/ajot.2024.050398

Dohle, C., Püllen, J., Nakaten, A., Küst, J., Rietz, C., & Karbe, H. (2009). Mirror Therapy Promotes Recovery From Severe Hemiparesis: A Randomized Controlled Trial. *Neurorehabilitation and Neural Repair*, *23*(3), 209-217. https://doi.org/10.1177/1545968308324786

Dyck, P. J., Boes, C. J., Mulder, D., Millikan, C., Windebank, A. J., Dyck, P. J. B., & Espinosa, R. (2005). History of standard scoring, notation, and summation of neuromuscular signs. A current survey and recommendation. *Journal of the Peripheral Nervous System*, *10*(2), 158-173.

Eickhoff, S., Heim, S., Zilles, K., & Amunts, K. (2006). Testing anatomically specified hypotheses in functional imaging using cytoarchitectonic maps. *NeuroImage*, *32*(2), 570-582. https://doi.org/10.1016/j.neuroimage.2006.04.204

Eickhoff, S. B., Paus, T., Caspers, S., Grosbras, M.-H., Evans, A. C., Zilles, K., & Amunts, K. (2007). Assignment of functional activations to probabilistic cytoarchitectonic areas revisited. [Review]. *NeuroImage*, *36*(3), 511-521. https://doi.org/10.1016/j.neuroimage.2007.03.060

Ertelt, D., Small, S., Solodkin, A., Dettmers, C., McNamara, A., Binkofski, F., & Buccino, G. (2007). Action observation has a positive impact on rehabilitation of motor deficits after stroke. *NeuroImage*, *36*, T164-T173. https://doi.org/https://doi.org/10.1016/j.neuroimage.2007.03.043

Esteban, O., Markiewicz, C. J., Blair, R. W., Moodie, C. A., Isik, A. I., Erramuzpe, A., Kent, J. D., Goncalves, M., DuPre, E., & Snyder, M. (2019). fMRIPrep: a robust preprocessing pipeline for functional MRI. *Nature methods*, *16*(1), 111-116.

Finn, E. S., Glerean, E., Hasson, U., & Vanderwal, T. (2022). Naturalistic imaging: The use of ecologically valid conditions to study brain function. *NeuroImage*, *247*, 118776. https://doi.org/10.1016/j.neuroimage.2021.118776

Finn, E. S., Glerean, E., Khojandi, A. Y., Nielson, D., Molfese, P. J., Handwerker, D. A., & Bandettini, P. A. (2020). Idiosynchrony: From shared responses to individual differences during naturalistic neuroimaging. *NeuroImage*, *215*, 116828. https://doi.org/10.1016/j.neuroimage.2020.116828

Fonov, V. S., Evans, A. C., McKinstry, R. C., Almli, C. R., & Collins, D. (2009). Unbiased nonlinear average age-appropriate brain templates from birth to adulthood. *NeuroImage*, *47*, S102.

Freud, E., Macdonald, S. N., Chen, J., Quinlan, D. J., Goodale, M. A., & Culham, J. C. (2018). Getting a grip on reality: Grasping movements directed to real objects and images rely on dissociable neural representations. *Cortex*, *98*, 34-48. https://doi.org/10.1016/j.cortex.2017.02.020

Frey, S. H., Funnell, M. G., Gerry, V. E., & Gazzaniga, M. S. (2005). A dissociation between the representation of tool-use skills and hand dominance: insights from left-and right-handed callosotomy patients. *Journal of Cognitive Neuroscience*, *17*(2), 262-272.

Gorgolewski, K., Burns, C. D., Madison, C., Clark, D., Halchenko, Y. O., Waskom, M. L., & Ghosh, S. S. (2011). Nipype: a flexible, lightweight and extensible neuroimaging data processing framework in python. *Frontiers in neuroinformatics*, *5*, 13. https://doi.org/https://doi.org/10.3389/fninf.2011.00013

Grady, C. L., Rieck, J. R., Nichol, D., Rodrigue, K. M., & Kennedy, K. M. (2020). Influence of sample size and analytic approach on stability and interpretation of brain-behavior correlations in task-related fMRI data. *Human Brain Mapping*, *42*(1), 204-219. https://doi.org/10.1002/hbm.25217

Greve, D. N., & Fischl, B. (2009). Accurate and robust brain image alignment using boundary-based registration. [Evaluation Study]. *NeuroImage*, *48*(1), 63-72. https://doi.org/10.1016/j.neuroimage.2009.06.060

Haaland, K. Y., Elsinger, C. L., Mayer, A. R., Durgerian, S., & Rao, S. M. (2004). Motor sequence complexity and performing hand produce differential patterns of hemispheric lateralization. *Cognitive Neuroscience, Journal of*, *16*(4), 621-636. http://ieeexplore.ieee.org/xpls/abs_all.jsp?arnumber=6789895

Haberling, I. S., Corballis, P. M., & Corballis, M. C. (2016). Language, gesture, and handedness: Evidence for independent lateralized networks. *Cortex*, *82*, 72-85. https://doi.org/10.1016/j.cortex.2016.06.003

Harris, P. A., Taylor, R., Thielke, R., Payne, J., Gonzalez, N., & Conde, J. G. (2009). Research electronic data capture (REDCap)—a metadata-driven methodology and workflow process for providing translational research informatics support. *Journal of biomedical informatics*, *42*(2), 377-381. https://doi.org/10.1016/j.jbi.2008.08.010

Hasson, U., Malach, R., & Heeger, D. J. (2010). Reliability of cortical activity during natural stimulation. *Trends in Cognitive Sciences*, *14*(1), 40-48. https://doi.org/10.1016/j.tics.2009.10.011

Hayashi, M. J., Saito, D. N., Aramaki, Y., Asai, T., Fujibayashi, Y., & Sadato, N. (2008). Hemispheric asymmetry of frequency-dependent suppression in the ipsilateral primary motor cortex during finger movement: a functional magnetic resonance imaging study. *Cereb Cortex*, *18*(12), 2932-2940. https://doi.org/10.1093/cercor/bhn053

He, B., Zhu, Z., Zhu, Q., Zhou, X., Zheng, C., Li, P., Zhu, S., Liu, X., & Zhu, J. (2014). Factors predicting sensory and motor recovery after the repair of upper limb peripheral nerve injuries [Research and Report]. *Neural Regeneration Research*, *9*(6), 661-672. https://doi.org/10.4103/1673-5374.130094

Jastorff, J., Clavagnier, S., Gergely, G., & Orban, G. A. (2010). Neural Mechanisms of Understanding Rational Actions: Middle Temporal Gyrus Activation by Contextual Violation. *Cerebral Cortex*, *21*(2), 318-329. https://doi.org/10.1093/cercor/bhq098

Jenkinson, M., Bannister, P., Brady, M., & Smith, S. (2002). Improved optimization for the robust and accurate linear registration and motion correction of brain images. *NeuroImage*, *17*(2), 825-841.

Jenkinson, M., Beckmann, C. F., Behrens, T. E. J., Woolrich, M. W., & Smith, S. M. (2012). FSL. *NeuroImage*, *62*(2), 782-790. https://doi.org/https://doi.org/10.1016/j.neuroimage.2011.09.015

Karimpoor, M., Churchill, N. W., Tam, F., Fischer, C. E., Schweizer, T. A., & Graham, S. J. (2018). Functional MRI of Handwriting Tasks: A Study of Healthy Young Adults Interacting with a Novel Touch-Sensitive Tablet. *Front Hum Neurosci*, *12*, 30. https://doi.org/10.3389/fnhum.2018.00030

Karimpoor, M., Tam, F., Strother, S. C., Fischer, C. E., Schweizer, T. A., & Graham, S. J. (2015). A computerized tablet with visual feedback of hand position for functional magnetic resonance imaging. *Frontiers in Human Neuroscience*, *9*, 150.

Kim, S. G., Ashe, J., Hendrich, K., Ellermann, J. M., Merkle, H., Uğurbil, K., & Georgopoulos, A. P. (1993). Functional magnetic resonance imaging of motor cortex: hemispheric asymmetry and handedness. *Science*, *261*(5121), 615-617. https://doi.org/10.1126/science.8342027

Kim, T., Fletcher, S., Gonzalez, C. L. R., & Philip, B. A. (2025). Block Building Task Identifies Distinct Groups of Left/Right-hand Choice Patterns After Unilateral Peripheral Nerve Injury. *J Vis Exp*(217). https://doi.org/10.3791/66919

Kim, T., Gassass, S., Carter, A. R., Dobbins, I. G., Liu, L., McAvoy, M., Sun, Z., Wang, Y., & Philip, B. A. (2023). *Ipsilateral parietal cortex supports precision movement with the non-dominant hand* Progress in Clinical Motor Control II, Chicago, IL.

Kim, T., Lohse, K. R., Mackinnon, S. E., & Philip, B. A. (2024). Patient Outcomes After Peripheral Nerve Injury Depend on Bimanual Dexterity and Preserved Use of the Affected Hand. *Neurorehabilitation and Neural Repair*, *38*(2), 134-147. https://doi.org/10.1177/15459683241227222

Kitchen, N. M., Dexheimer, B., Yuk, J., Maenza, C., Ruelos, P. R., Kim, T., & Sainburg, R. L. (2025). The complementary dominance hypothesis: a model for remediating the 'good' hand in stroke survivors. *Journal of Physiology*, *603*(3), 663-683. https://doi.org/10.1113/JP285561

Klein, A., Ghosh, S. S., Bao, F. S., Giard, J., Häme, Y., Stavsky, E., Lee, N., Rossa, B., Reuter, M., & Chaibub Neto, E. (2017). Mindboggling morphometry of human brains. *PLoS Computational Biology*, *13*(2), e1005350.

Kornysheva, K., & Diedrichsen, J. (2014). Human premotor areas parse sequences into their spatial and temporal features. *Elife*, *3*, e03043. https://doi.org/10.7554/eLife.03043

Kriegeskorte, N., Simmons, W. K., Bellgowan, P. S., & Baker, C. I. (2009). Circular analysis in systems neuroscience: the dangers of double dipping. *Nat Neurosci*, *12*(5), 535-540. https://doi.org/10.1038/nn.2303

Kringelbach, M. L., Perl, Y. S., Tagliazucchi, E., & Deco, G. (2023). Toward naturalistic neuroscience: Mechanisms underlying the flattening of brain hierarchy in movie-watching compared to rest and task. *Science Advances*, *9*(2), eade6049. https://doi.org/doi:10.1126/sciadv.ade6049

Liepmann, H. M. O. (1905). Die linke Hemisphäre und das Handeln. Münchener Medizinische Wochenschrift. (49), 2322–2326, 2375–2378.

Liesefeld, H. R., & Janczyk, M. (2023). Same same but different: Subtle but consequential differences between two measures to linearly integrate speed and accuracy (LISAS vs. BIS). *Behav Res Methods*, *55*(3), 1175-1192. https://doi.org/10.3758/s13428-022-01843-2

Lindenberg, R., Renga, V., Zhu, L. L., Nair, D., & Schlaug, G. (2010). Bihemispheric brain stimulation facilitates motor recovery in chronic stroke patients. *Neurology*, *75*(24), 2176-2184. https://doi.org/10.1212/wnl.0b013e318202013a

Mani, S., Mutha, P. K., Przybyla, A., Haaland, K. Y., Good, D. C., & Sainburg, R. L. (2013). Contralesional motor deficits after unilateral stroke reflect hemisphere-specific control mechanisms. *Brain*, *136*(Pt 4), 1288-1303. https://doi.org/10.1093/brain/aws283

Marcori, A. J., Monteiro, P. H. M., & Okazaki, V. H. A. (2019). Changing handedness: What can we learn from preference shift studies? *Neurosci Biobehav Rev*, *107*, 313-319. https://doi.org/10.1016/j.neubiorev.2019.09.019

Masharipov, R., Knyazeva, I., Korotkov, A., Cherednichenko, D., & Kireev, M. (2024). Comparison of whole-brain task-modulated functional connectivity methods for fMRI task connectomics. *Commun Biol*, *7*. https://doi.org/10.1101/2024.01.22.576622

Mathiowetz, V., Volland, G., Kashman, N., & Weber, K. (1985). Adult norms for the Box and Block Test of manual dexterity. *American Journal of Occupational Therapy*, *39*(6), 386-391.

McLaren, D. G., Ries, M. L., Xu, G., & Johnson, S. C. (2012). A generalized form of context-dependent psychophysiological interactions (gPPI): a comparison to standard approaches. *NeuroImage*, *61*(4), 1277-1286. https://doi.org/10.1016/j.neuroimage.2012.03.068

Mumford, J. A. (2012). A power calculation guide for fMRI studies. *Soc Cogn Affect Neurosci*, *7*(6), 738-742. https://doi.org/10.1093/scan/nss059

Mumford, J. A. (2017). *FEAT registration workaround*. Retrieved June 1 from https://mumfordbrainstats.tumblr.com/post/166054797696/feat-registration-workaround

Nieto-Castanon, A. (2020). *Handbook of functional connectivity Magnetic Resonance Imaging methods in CONN*. https://doi.org/10.56441/hilbertpress.2207.6598

Nojima, I., Mima, T., Koganemaru, S., Thabit, M. N., Fukuyama, H., & Kawamata, T. (2012). Human Motor Plasticity Induced by Mirror Visual Feedback. *The Journal of Neuroscience*, *32*(4), 1293-1300. https://doi.org/10.1523/jneurosci.5364-11.2012

Oldfield, R. C. (1971). The assessment and analysis of handedness: the Edinburgh inventory. *Neuropsychologia*, *9*(1), 97-113. https://doi.org/https://doi.org/10.1016/0028-3932(71)90067-4

Patriat, R., Reynolds, R. C., & Birn, R. M. (2017). An improved model of motion-related signal changes in fMRI. *NeuroImage*, *144*, 74-82.

Peterson, S. M., Singh, S. H., Wang, N. X. R., Rao, R. P. N., & Brunton, B. W. (2021). Behavioral and Neural Variability of Naturalistic Arm Movements. *eneuro*, *8*(3). https://doi.org/10.1523/ENEURO.0007-21.2021

Philip, B. A., & Frey, S. H. (2014). Compensatory Changes Accompanying Chronic Forced Use of the Nondominant Hand by Unilateral Amputees. *The Journal of Neuroscience: the Official Journal of the Society for Neuroscience*, *34*(10), 3622-3631. https://doi.org/10.1523/JNEUROSCI.3770-13.2014

Philip, B. A., & Frey, S. H. (2016). Increased functional connectivity between cortical hand areas and praxis network associated with training-related improvements in non-dominant hand precision drawing. *Neuropsychologia*, *87*, 157-168. https://doi.org/10.1016/j.neuropsychologia.2016.05.016

Philip, B. A., Kaskutas, V., & Mackinnon, S. E. (2020). Impact of handedness on disability after unilateral upper extremity peripheral nerve disorder. *HAND*, *15*(3), 327-334. https://doi.org/https://doi.org/10.1177/1558944718810880

Philip, B. A., Li, F., Hawkins-Chernof, E., Swamidass, V., & Zwir, I. (2023). Motor Assessment With the STEGA iPad App to Measure Handwriting in Children. *American Journal of Occupational Therapy*, *77*(3).

Philip, B. A., McAvoy, M. P., & Frey, S. H. (2021). Interhemispheric Parietal-Frontal Connectivity Predicts the Ability to Acquire a Nondominant Hand Skill. *Brain Connectivity*, *11*(4). https://doi.org/10.1089/brain.2020.0916

Pool, E. M., Rehme, A. K., Fink, G. R., Eickhoff, S. B., & Grefkes, C. (2014). Handedness and effective connectivity of the motor system. *NeuroImage*, *99*, 451-460. https://doi.org/10.1016/j.neuroimage.2014.05.048

Potgieser, A. R., van der Hoorn, A., & de Jong, B. M. (2015). Cerebral activations related to writing and drawing with each hand. *PLoS ONE*, *10*(5), e0126723. https://doi.org/10.1371/journal.pone.0126723

Power, J. D., Barnes, K. A., Snyder, A. Z., Schlaggar, B. L., & Petersen, S. E. (2012). Spurious but systematic correlations in functional connectivity MRI networks arise from subject motion. *NeuroImage*, *59*(3), 2142-2154. https://doi.org/10.1016/j.neuroimage.2011.10.018

Power, J. D., Mitra, A., Laumann, T. O., Snyder, A. Z., Schlaggar, B. L., & Petersen, S. E. (2014). Methods to detect, characterize, and remove motion artifact in resting state fMRI. *NeuroImage*, *84*, 320-341.

Ras, M., Wyrwa, M., Stachowiak, J., Buchwald, M., Nowik, A. M., & Kroliczak, G. (2022). Complex tools and motor-to-mechanical transformations. *Sci Rep*, *12*(1), 8041. https://doi.org/10.1038/s41598-022-12142-3

Reddy, N. A., Zvolanek, K. M., Moia, S., Caballero-Gaudes, C., & Bright, M. G. (2024). Denoising task-correlated head motion from motor-task fMRI data with multi-echo ICA. *Imaging Neuroscience*, *2*. https://doi.org/10.1162/imag_a_00057

Rosenzopf, H., Wiesen, D., Basilakos, A., Yourganov, G., Bonilha, L., Rorden, C., Fridriksson, J., Karnath, H. O., & Sperber, C. (2022). Mapping the human praxis network: an investigation of white matter disconnection in limb apraxia of gesture production. *Brain Commun*, *4*(1), fcac004. https://doi.org/10.1093/braincomms/fcac004

Saarimaki, H. (2021). Naturalistic Stimuli in Affective Neuroimaging: A Review. *Front Hum Neurosci*, *15*, 675068. https://doi.org/10.3389/fnhum.2021.675068

Sainburg, R. L. (2002). Evidence for a dynamic-dominance hypothesis of handedness. *Experimental brain research Experimentelle Hirnforschung Expérimentation cérébrale*, *142*(2), 241-258. https://doi.org/10.1007/s00221-001-0913-8

Sainburg, R. L. (2014). Convergent models of handedness and brain lateralization. *Frontiers in Psychology*, *5*. https://doi.org/10.3389/fpsyg.2014.01092

Satterthwaite, T. D., Elliott, M. A., Gerraty, R. T., Ruparel, K., Loughead, J., Calkins, M. E., Eickhoff, S. B., Hakonarson, H., Gur, R. C., & Gur, R. E. (2013). An improved framework for confound regression and filtering for control of motion artifact in the preprocessing of resting-state functional connectivity data. *NeuroImage*, *64*, 240-256.

Scarapicchia, V., Brown, C., Mayo, C., & Gawryluk, J. R. (2017). Functional Magnetic Resonance Imaging and Functional Near-Infrared Spectroscopy: Insights from Combined Recording Studies. *Front Hum Neurosci*, *11*, 419. https://doi.org/10.3389/fnhum.2017.00419

Schaefer, S. Y., Haaland, K. Y., & Sainburg, R. L. (2009). Hemispheric specialization and functional impact of ipsilesional deficits in movement coordination and accuracy. *Neuropsychologia*, *47*(13), 2953-2966. https://doi.org/10.1016/j.neuropsychologia.2009.06.025

Schaefer, S. Y., Mutha, P. K., Haaland, K. Y., & Sainburg, R. L. (2012). Hemispheric specialization for movement control produces dissociable differences in online corrections after stroke. *Cereb Cortex*, *22*(6), 1407-1419. https://doi.org/10.1093/cercor/bhr237

Schluter, N. D., Rushworth, M. F., Passingham, R. E., & Mills, K. R. (1998). Temporary interference in human lateral premotor cortex suggests dominance for the selection of movements. A study using transcranial magnetic stimulation. *Brain*, *121 (Pt 5)*, 785-799. https://doi.org/10.1093/brain/121.5.785

Seidman, L. J., Faraone, S. V., Goldstein, J. M., Goodman, J. M., Kremen, W. S., Toomey, R., Tourville, J., Kennedy, D., Makris, N., & Caviness, V. S. (1999). Thalamic and amygdala–hippocampal volume reductions in first-degree relatives of patients with schizophrenia: an MRI-based morphometric analysis. *Biological Psychiatry*, *46*(7), 941-954.

Shabbott, B. A., & Sainburg, R. L. (2008). Differentiating between two models of motor lateralization. *J Neurophysiol*, *100*(2), 565-575. https://doi.org/10.1152/jn.90349.2008

Shabbott, B. A., & Sainburg, R. L. (2008). Differentiating between two models of motor lateralization. *Journal of Neurophysiology*, *100*(2), 565-575. https://doi.org/10.1152/jn.90349.2008

Sharma, N., Pomeroy, V. M., & Baron, J.-C. (2006). Motor Imagery. *Stroke*, *37*(7), 1941-1952. https://doi.org/10.1161/01.str.0000226902.43357.fc

Singh-Curry, V., & Husain, M. (2009). The functional role of the inferior parietal lobe in the dorsal and ventral stream dichotomy. *Neuropsychologia*, *47*(6), 1434-1448. https://doi.org/10.1016/j.neuropsychologia.2008.11.033

Smith, J. C., & Frey, S. H. (2011, Feb 09). *Use of independent component analysis to define regions of interest for fMRI studies*. International Society for Magnetic Resonance in Medicine (ISMRM), Montreal, Canada. https://archive.ismrm.org/2011/1618.html

Smith, S. M., Jenkinson, M., Woolrich, M. W., Beckmann, C. F., Behrens, T. E. J., Johansen-Berg, H., Bannister, P. R., De Luca, M., Drobnjak, I., Flitney, D. E., Niazy, R. K., Saunders, J., Vickers, J., Zhang, Y., De Stefano, N., Brady, J. M., & Matthews, P. M. (2004). Advances in functional and structural MR image analysis and implementation as FSL. [Review]. *NeuroImage*, *23 Suppl 1*, S208-219. https://doi.org/10.1016/j.neuroimage.2004.07.051

Stinear, C. M., Barber, P. A., Petoe, M., Anwar, S., & Byblow, W. D. (2012). The PREP algorithm predicts potential for upper limb recovery after stroke. *Brain*, *135*(8), 2527-2535. https://doi.org/10.1093/brain/aws146

Stinear, C. M., & Byblow, W. D. (2004). Impaired modulation of intracortical inhibition in focal hand dystonia. *Cereb Cortex*, *14*(5), 555-561. https://doi.org/10.1093/cercor/bhh017

Tam, F., Churchill, N. W., Strother, S. C., & Graham, S. J. (2011). A new tablet for writing and drawing during functional MRI. *Human Brain Mapping*, *32*(2), 240-248.

Tsurugizawa, T., Taki, A., Zalesky, A., & Kasahara, K. (2023). Increased interhemispheric functional connectivity during non-dominant hand movement in right-handed subjects. *iScience*, *26*(9), 107592. https://doi.org/10.1016/j.isci.2023.107592

Tustison, N. J., Avants, B. B., Cook, P. A., Zheng, Y., Egan, A., Yushkevich, P. A., & Gee, J. C. (2010). N4ITK: improved N3 bias correction. *IEEE transactions on medical imaging*, *29*(6), 1310-1320.

Tzourio-Mazoyer, N., Petit, L., Zago, L., Crivello, F., Vinuesa, N., Joliot, M., Jobard, G., Mellet, E., & Mazoyer, B. (2015). Between-hand difference in ipsilateral deactivation is associated with hand lateralization: fMRI mapping of 284 volunteers balanced for handedness. *Front Hum Neurosci*, *9*, 5. https://doi.org/10.3389/fnhum.2015.00005

Uomini, N. T. (2009). The prehistory of handedness: archaeological data and comparative ethology. *Journal of Human Evolution*, *57*(4), 411-419.

Uomini, N. T., & Ruck, L. (2018). Manual laterality and cognition through evolution: An archeological perspective. *Prog Brain Res*, *238*, 295-323. https://doi.org/10.1016/bs.pbr.2018.06.015

Valyear, K. F., & Frey, S. H. (2015). Human posterior parietal cortex mediates hand-specific planning. *NeuroImage*, *114*, 226-238. https://doi.org/10.1016/j.neuroimage.2015.03.058

van Kemenade, B. M., Arikan, B. E., Podranski, K., Steinstrater, O., Kircher, T., & Straube, B. (2019). Distinct Roles for the Cerebellum, Angular Gyrus, and Middle Temporal Gyrus in Action-Feedback Monitoring. *Cereb Cortex*, *29*(4), 1520-1531. https://doi.org/10.1093/cercor/bhy048

Vandierendonck, A. (2021). On the Utility of Integrated Speed-Accuracy Measures when Speed-Accuracy Trade-off is Present. *J Cogn*, *4*(1), 22. https://doi.org/10.5334/joc.154

Versace, E., & Vallortigara, G. (2015). Forelimb preferences in human beings and other species: multiple models for testing hypotheses on lateralization. *Front Psychol*, *6*, 233. https://doi.org/10.3389/fpsyg.2015.00233

Verstynen, T., Diedrichsen, J., Albert, N., Aparicio, P., & Ivry, R. B. (2005). Ipsilateral motor cortex activity during unimanual hand movements relates to task complexity. *J Neurophysiol*, *93*(3), 1209-1222. https://doi.org/10.1152/jn.00720.2004

Vingerhoets, G., Acke, F., Alderweireldt, A.-S., Nys, J., Vandemaele, P., & Achten, E. (2012). Cerebral lateralization of praxis in right- and left-handedness: Same pattern, different strength. *Human Brain Mapping*, *33*(4), 763-777. https://doi.org/https://doi.org/10.1002/hbm.21247

Vingerhoets, G., Verhelst, H., Gerrits, R., Badcock, N., Bishop, D. V., Carey, D., Flindall, J., Grimshaw, G., Harris, L. J., & Hausmann, M. (2023). Laterality indices consensus initiative (LICI): A Delphi expert survey report on recommendations to record, assess, and report asymmetry in human behavioural and brain research. *Laterality*, *28*(2-3), 122-191.

Wang, J., & Sainburg, R. L. (2007). The dominant and nondominant arms are specialized for stabilizing different features of task performance. *Experimental brain research Experimentelle Hirnforschung Expérimentation cérébrale*, *178*(4), 565-570. https://doi.org/10.1007/s00221-007-0936-x

Wang, J., Tian, Y., Wang, M., Cao, L., Wu, H., Zhang, Y., Wang, K., & Jiang, T. (2016). A lateralized top-down network for visuospatial attention and neglect. *Brain Imaging Behav*, *10*(4), 1029-1037. https://doi.org/10.1007/s11682-015-9460-y

Waters-Metenier, S., Husain, M., Wiestler, T., & Diedrichsen, J. (2014). Bihemispheric Transcranial Direct Current Stimulation Enhances Effector-Independent Representations of Motor Synergy and Sequence Learning. *The Journal of Neuroscience*, *34*(3), 1037-1050. https://doi.org/10.1523/jneurosci.2282-13.2014

Wheaton, L., Fridman, E., Bohlhalter, S., Vorbach, S., & Hallett, M. (2009). Left parietal activation related to planning, executing and suppressing praxis hand movements. *Clinical Neurophysiology*, *120*(5), 980-986.

Wischnewski, M., Kowalski, G. M., Rink, F., Belagaje, S. R., Haut, M. W., Hobbs, G., & Buetefisch, C. M. (2016). Demand on skillfulness modulates interhemispheric inhibition of motor cortices. *Journal of Neurophysiology*, *115*(6), 2803-2813. https://doi.org/10.1152/jn.01076.2015

Wolpert, D. M., Goodbody, S. J., & Husain, M. (1998). Maintaining internal representations: the role of the human superior parietal lobe. *Nature neuroscience*, *1*(6), 529-533. http://www.nature.com/neuro/journal/v1/n6/abs/nn1098_529.html

Yang, Y., Li, J., Zhao, K., Tam, F., Graham, S. J., Xu, M., & Zhou, K. (2024). Lateralized Functional Connectivity of the Sensorimotor Cortex and its Variations During Complex Visuomotor Tasks. *The Journal of Neuroscience: the Official Journal of the Society for Neuroscience*, *44*(5). https://doi.org/10.1523/JNEUROSCI.0723-23.2023

Zhang, Y., Brady, M., & Smith, S. (2002). Segmentation of brain MR images through a hidden Markov random field model and the expectation-maximization algorithm. *IEEE transactions on medical imaging*, *20*(1), 45-57.

Zhang, Y., Kim, J.-H., Brang, D., & Liu, Z. (2021). Naturalistic stimuli: A paradigm for multiscale functional characterization of the human brain. *Current Opinion in Biomedical Engineering*, *19*, 100298. https://doi.org/https://doi.org/10.1016/j.cobme.2021.100298